Single-atom mirror for one-dimensional atomic lattice gases

A. Micheli and P. Zoller

Institute for Theoretical Physics, University of Innsbruck, and Institute for Quantum Optics and Quantum Information of the Austrian Academy of Sciences, A-6020 Innsbruck, Austria

(Received 20 June 2005; revised manuscript received 19 January 2006; published 20 April 2006)

We propose a scheme utilizing quantum interference to control the transport of atoms in a one-dimensional optical lattice by a single impurity atom. The two internal state of the impurity represent a spin-1/2 (qubit), which in one spin state is perfectly transparent to the lattice gas, and in the other spin state acts as a single atom mirror, confining the lattice gas. This allows one to "amplify" the state of the qubit, and provides a single-shot quantum nondemolition measurement of the state of the qubit. We derive exact analytical expression for the scattering of a single atom by the impurity, and give approximate expressions for the dynamics of a gas of many interacting bosonic or fermionic atoms.

DOI: 10.1103/PhysRevA.73.043613 PACS number(s): 03.75.Lm, 42.50.−p, 03.67.Lx

I. INTRODUCTION

One of the fundamental models in quantum optics is the interaction of a spin-1/2 system with a bosonic mode [1]. The most prominent example is cavity quantum electrodynamics (CQED), where a two level atom interacts with a single mode of the radiation field in a high-Q cavity. CQED has been the topic of a series of seminal experiments both in the microwave and optical regime, demonstrating quantum control on the level of single atoms and photons in an open quantum system [2–5].

In the present paper we will consider a system with the same basic ingredients, however, in the context of cold atoms and quantum degenerate gases. The key feature of these systems is their controllability and weak decoherence. In particular we employ two aspects of control, the confinement of atoms in optical lattices [6–9] and (magnetic or optical) Feshbach resonances as a way to manipulate atomic interactions [10–13]. According to the setup described in Fig. 1(a) we will study the dynamics of an atomic quantum gas in one dimension (1D) (with a single internal atomic state), representing bosonic or fermionic "modes," controlled by an atomic spin-1/2 impurity. The quantum gas is confined by tight trapping potentials (e.g., an optical or magnetic trap), so that only the motional degrees along the z axis in Fig. 1(a) are relevant. In the z direction the motion is confined to the left by a trapping potential (e.g., a blue sheet of light), while the atomic impurity restricts the motion of the gas to the right due to collisional interactions of the quantum gas with the impurity. The atom representing the impurity can, for example, be a different atomic species in a tight trapping potential, a configuration discussed in Refs. [14,15] as an atomic quantum dot (0D system). Thus the impurity atom plays the role of "single-atom mirror" confining the quantum gas in an "atomic cavity."

In our model system the impurity atom is an internal two level system, which we write as an effective spin-1/2. In the following we will also interpret this two-level system as a qubit with two logical states $|0\rangle=|\downarrow\rangle$ and $|1\rangle=|\uparrow\rangle$. Cold atom collision physics allows for a situation where the collisional properties (scattering length) of the impurity atom and atoms in the quantum gas are spin-dependent. As illustrated in Fig. 1(a), we assume that in one spin state, say $|\downarrow\rangle$, the single impurity atom is completely transparent for the quantum gas, i.e., the gas will leak out through the "mirror." In contrast, in the other spin state the mirror atom is "highly reflective" confining the gas. For an impurity atom (qubit) initially prepared in a spin superposition

$$|\psi_Q(t=0)\rangle = \alpha_\uparrow|\uparrow\rangle + \alpha_\downarrow|\downarrow\rangle$$

the combined system at a time t will be in a macroscopic superposition state

$$|\Psi(t)\rangle = \alpha_\uparrow|\uparrow\rangle|\phi_\uparrow(t)\rangle + \alpha_\downarrow|\downarrow\rangle|\phi_\downarrow(t)\rangle. \quad (1)$$

with $|\phi_\sigma(t)\rangle$ many body wave functions of the gas atoms. Thus $|\Psi(t)\rangle$ represents a Schrödinger cat state of two entangled quantum phases of gas atoms, the first one corresponding to gas confined by the mirror [Fig. 1(a), upper figure] and the second one to the expanding gas [Fig. 1(a), lower figure]. The entanglement of the spin with a macroscopic number of atoms can be interpreted as a macroscopic quantum gate, as explained in Fig. 2, implementing a quantum nondemolition interaction (QND) [16]. In this sense the setup represents an "amplifier" of the state of the qubit. This

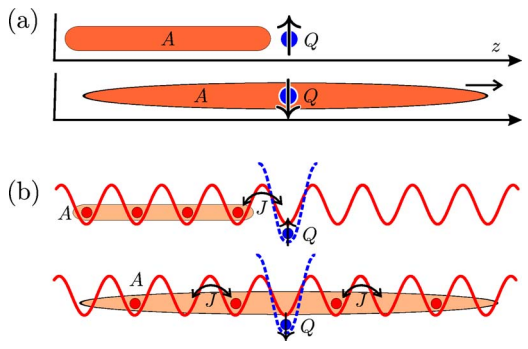

FIG. 1. (Color online) (a) A spin-1/2 impurity Q used as a switch: in one spin state it is transparent to the probe atoms A, but in the other it acts as a single atom mirror. (b) Implementation of the SAT: The impurity atom Q and the probe atoms A are trapped separately in state-dependent 1D optical lattices. The probe atoms A initially are in a Mott insulating state.

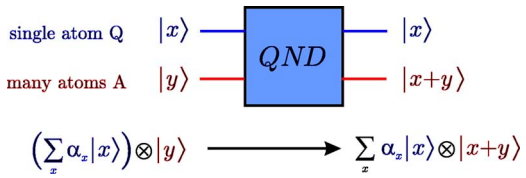

FIG. 2. (Color online) The single atom mirror as a macroscopic quantum gate. The qubit Q entangles two distinguishable macroscopic phase of the probe atoms A and provides for a quantum nondemolition interaction.

situation is reminiscent of a single electron transistor (SET) in mesoscopic physics [17], and has stimulated the name single atom transistor (SAT) for the setup Fig. 1(a) in Ref. [18], with the essential difference that the dynamics underlying (1) is completely coherent. We finally remark that this setup also allows for a single shot QND measurement of the impurity atom (qubit) by observing in a single experiment the distinct properties of the $|\phi_\downarrow(t)\rangle$ or $|\phi_\uparrow(t)\rangle$ quantum phases.

As a variant of the configuration of Fig. 1(a) we will consider below in particular the case where the quantum gas is loaded in an optical lattice, as illustrated in Fig. 1(b). In this case the gas could be loaded initially, for example, in a Mott insulating state, i.e., where large repulsion of the gas atom leads to a filling of the lattice sites with exactly one atom per lattice site [7,9,19]. The cat state (1) will thus correspond to a superposition of the Mott phase and the melted Mott phase, i.e., a (quasi) condensate of atoms obtained by expansion of the atomic gas

$$|\Psi(t)\rangle = \alpha_\downarrow|\downarrow\rangle|\mathrm{BEC}\rangle + \alpha_\uparrow|\uparrow\rangle|\mathrm{Mott}\rangle. \tag{2}$$

In this case the distinguishing features of the two entangled quantum phases are the observation or nonobservation of interference fringes as signatures of the Mott and BEC phase, when the atomic gas in released in a single experiment.

Transport through an impurity is a well studied problem in mesoscopic condensed matter physics [20–23], which typically focuses on conductance properties of a system attached to leads. In contrast, in the context of cold gases we have a full time-dependent coherent dynamics in an otherwise closed system.

A short summary of the present work including results from numerical studies was presented in Ref. [18]. In this paper we will present details of our analytical calculations, while we refer to Ref. [24] on a complementary numerical treatment of these problems using time-dependent DMRG techniques.

The paper is organized as follows. In Sec. II we introduce the model used for describing the implementation of the single atom mirror using cold atoms in optical lattice. In Sec. III we consider the detailed scattered processes involved in the transport of a single particle through the mirror. We solve exactly the scattering problem in the lattice by integrating the Lippmann-Schwinger Equation (LSE) and discuss the obtained scattering amplitudes and spectrum of the bound states. Finally, in Sec. IV we generalize the discussion to the case of interacting many-systems including the cases of a 1D degenerate Fermi-gas, a 1D quasicondensate, and a Tonks gas.

II. MODEL

In this section we introduce the our model system by specifying the Hamiltonian for a 1D lattice gas coupled to an impurity, and we explain the key idea behind our setup. We will start with a discussion of spin-dependent collisions between the gas and the impurity, and then present the central idea of quantum interference as a way to switch atomic transport.

A. Effective spin-dependent Hamiltonian

We consider the dynamics of a spin-1/2 atomic impurity Q coupled to a 1D quantum gas of either bosonic or fermionic probe atoms A. The Hamiltonian for system is split into three parts as

$$H = H_A + H_Q + H_{AQ}. \tag{3}$$

Here H_Q (H_A) describes the uncoupled dynamics of the impurity atom Q (the degenerate quantum gas of probe atoms A), while H_{AQ} accounts for the interaction between the two atomic species Q and A.

A degenerate quantum gas of bosonic or fermionic atoms A trapped in the lowest band of a 1D optical lattice is well described by a Hubbard model [6]

$$H_A = \sum_j E_{A,j} a_j^\dagger a_j - J\sum_j (a_j^\dagger a_{j+1} + a_{j+1}^\dagger a_j) + \frac{U}{2}\sum_j a_j^\dagger a_j^\dagger a_j a_j, \tag{4}$$

where $a_j^\dagger$ (a_j) are the creation (annihilation) operators for an atom A on the site j, which obey standard commutation (anticommutation) relations for the case of bosonic (fermionic) atoms A. Moreover, $E_{A,j}$ account for the shift of the bare energy of an atom localized on the site j in the presence of an external (e.g., magnetic) shallow trap V_{ext}, J is the tunneling matrix element for neighboring sites, and U gives the collisional interaction, i.e., the onsite-shift for two atoms A localized within the same well (which would be zero for the case of fermions in the same internal state). Denoting the optical lattice potential for the atoms A by V_{opt}, their mass by m and their scattering-length by a_s, we have the local potentials $E_{j,A}$, the tunneling matrix element J and the onsite-shift U given by

$$E_{j,A} = \int d^3 r w_j(\mathbf{r})^* \left[-\frac{\hbar^2}{2m}\nabla^2 + V_{\mathrm{opt}}(\mathbf{r}) + V_{\mathrm{ext}}(\mathbf{r}) \right] w_j(\mathbf{r}),$$

$$J = \int d^3 r w_{j+1}(\mathbf{r})^* \left[-\frac{\hbar^2}{2m}\nabla^2 + V_{\mathrm{opt}}(\mathbf{r}) \right] w_j(\mathbf{r}),$$

$$U = \frac{4\pi\hbar^2 a_s}{m} \int d^3 r |w_j(\mathbf{r})|^4,$$

where $w_j(\mathbf{r})$ is the Wannier function for a particle localized on the site j.

In the present setup we regard the impurity atom Q to be trapped within a tight one-dimensional lattice, as depicted in Fig. 1(b). Therefore, we may restrict ourselves to the lowest trap-state of the $j=0$ well for the internal states $\sigma=\downarrow,\uparrow$, respectively. The uncoupled dynamics of the impurity corresponds to spin-1/2 system, i.e.,

$$H_Q = \sum_\sigma E_{Q,\sigma}|Q_\sigma\rangle\langle Q_\sigma|, \tag{5}$$

where $|Q_\sigma\rangle$ ($E_{Q,\sigma}$) denotes the state (energy) of the atom Q with spin $\sigma=\downarrow,\uparrow$.

Given the tight trapping of the impurity atom, the interaction of probe and impurity atom is restricted to the site of the impurity, and in general has the form of an effective spin-dependent collisional interaction

$$H_{AQ} = W_{\text{eff},\uparrow}|\uparrow\rangle\langle\uparrow|a_0^\dagger a_0 + W_{\text{eff},\downarrow}|\downarrow\rangle\langle\downarrow|a_0^\dagger a_0, \tag{6}$$

where $a_0^\dagger$ (a_0) is the creation (annihilation) operator for a probe atom on the site of the impurity, $j=0$. Here, $W_{\text{eff},\sigma}=4\pi\hbar^2 a_\sigma \int d^3r |w_0(\mathbf{r})|^2 |\psi_{Q,\sigma}(\mathbf{r})|^2/\mu$ denotes the effective interaction for a probe atom A and the impurity atom Q in state σ in terms of their effective scattering length a_σ and μ is the reduced mass for A and Q. The effective tunneling rate of a probe atom with energy E through the impurity is then given by $J_{\text{eff},\sigma}=J^2/(E-W_{\text{eff},\sigma})+O(J^4)$ for the qubit in state σ. An obvious way to provide for a spin-dependent single atom mirror is to have the effective interaction for one spin state as large as possible ($|W_{\text{eff},\uparrow}| \gg J$), thus blocking the transport of the probe atoms through the impurity site, while for the other it is effectively not present ($|W_{\text{eff},\downarrow}| \ll J$). This can be achieved, for example, by tuning the internal state dependent scattering length a_σ or by engineering the spin-dependent trapping [6]. The quality of the qubit dependent switch then depends on the difference of the moduli of the effective interactions, $|W_{\text{eff},\uparrow}|-|W_{\text{eff},\downarrow}|$. Thus the goal an efficient scheme is to make $|W_{\text{eff},\uparrow}|-|W_{\text{eff},\downarrow}|$ as large as possible and obtain $|W_{\text{eff},\uparrow}| \gg J \gg |W_{\text{eff},\downarrow}|$.

B. Controlling the transport by interference

In this section we will show now that with the help of quantum interference we can engineer an effectively infinite (zero) atomic repulsion, $W_{\text{eff},\uparrow}\to\infty$ ($W_{\text{eff},\downarrow}\to 0$), for the qubit in state $\sigma=\downarrow$ ($\sigma=\uparrow$). This is equivalent to tuning the Feshbach resonance to the point of infinite (zero) scattering length.

The quantum interference mechanism required to engineer the described spin dependence of $W_{\text{eff},\sigma}$ is obtained by exploiting the properties of either an optical or a magnetic Feshbach resonance. In the case of an optical Feshbach resonance a Raman laser drives the transitions from the joint state of the two atoms on the impurity site $a_0^\dagger|Q_\sigma\rangle \equiv |Q_\sigma\rangle \otimes a_0^\dagger|\text{vac}\rangle$, via an off-resonant excited molecular state back to a bound hetero-nuclear molecular state $|M_\sigma\rangle$ in the lowest electronic manifold (see Fig. 3). The Raman processes is described by the effective two-photon Rabi frequency Ω_σ and detuning Δ_σ for each spin component σ. For the case of a magnetic Feshbach resonance, the effective Hamiltonian

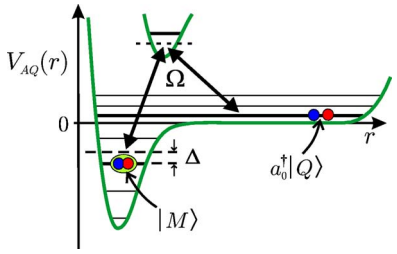

FIG. 3. (Color online) The optical Feshbach setup couples the atomic state $a_0^\dagger|Q\rangle$ (in a particular motional state quantized by the trap) to a molecular bound state $|M\rangle$ of the Born-Oppenheimer potential $V_{AQ}(r)$ with effective Rabi frequency Ω and detuning Δ.

has the same form, but with Ω_σ being the coupling strength between the open and closed channels and Δ_σ the detuning of the magnetic field. The Hamiltonian describing the interaction between the probe atoms and the impurity is [12]

$$H_{AQ} = \sum_\sigma [E_{M,\sigma}|M_\sigma\rangle\langle M_\sigma| + \Omega_\sigma(|M_\sigma\rangle\langle Q_\sigma|a_0 + \text{H.c.}) + W_{Q,\sigma}|Q_\sigma\rangle\langle Q_\sigma|a_0^\dagger a_0 + W_{M,\sigma}|M_\sigma\rangle\langle M_\sigma|a_0^\dagger a_0], \tag{7}$$

where the bare energy of the molecular bound state is $E_{M,\sigma}=E_{A,0}+E_{Q,\sigma}+\Delta_\sigma$. Here the first two terms describe the resonant coupling induced by the Feshbach mechanism, while the last two describe the off-resonant collisions between an atom A and an atom Q (a molecule M) in state σ by means of their on-site shift $W_{Q,\sigma}$ ($W_{M,\sigma}$) for the impurity site. The Hamiltonian (3) conserves the spin-component of the impurity $S_\sigma \equiv |Q_\sigma\rangle\langle Q_\sigma| + |M_\sigma\rangle\langle M_\sigma|$, i.e., $[H,S_\sigma]=0$. Therefore, we can consider the dynamics for the two spin components of Q separately, and in the following we will drop the spin index σ and choose the reference energy as $E_{A,0}=E_{Q,\sigma}=0$.

For off-resonant laser driving ($|\Delta| \gg \Omega$), the Feshbach resonance enhances the interaction between A and Q atoms, giving the familiar result $W_{\text{eff}}=W_Q+\Omega^2/\Delta$. However, for resonant driving ($\Delta=0$) the physical mechanism changes, and the effective tunneling J_{eff} of an atom A past the impurity (Fig. 4, I→III) is blocked by quantum interference. On the impurity site, laser driving mixes the states $a_0^\dagger|Q\rangle$ and $|M\rangle$, forming two dressed states with energies $E_\pm = W_Q/2 \pm (W_Q^2/4+\Omega^2)^{1/2}$ (Fig. 4, II). The two resulting paths for a particle of energy E destructively interfere so that for large $\Omega \gg J$ and $W_Q=0$,

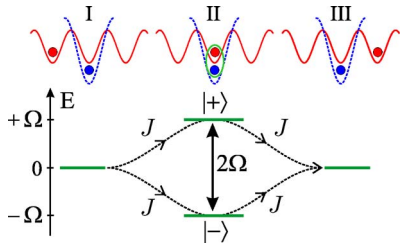

FIG. 4. (Color online) A single atom passes the impurity (I→III) via the two dressed states (II), $|+\rangle = a_0^\dagger|Q\rangle + |M\rangle$ and $|-\rangle = a_0^\dagger|Q\rangle - |M\rangle$ and quantum interference gives rise to an effective tunneling rate J_{eff}.

$$J_{\text{eff}} = -\frac{J^2}{E+\Omega} - \frac{J^2}{E-\Omega} \to 0.$$

This is analogous to the interference effect underlying electromagnetically induced transparency (EIT) [25], and is equivalent to having an effective interaction $W_{\text{eff}} \to \infty$. In addition, if we choose $\Delta = \Omega^2/W_Q$, the paths interfere constructively, screening the background interactions W_Q to produce perfect transmission ($W_{\text{eff}} \to 0$). The insensitivity of the interference scheme to losses from the dressed states due to their large detuning has been argued in Ref. [18].

III. SINGLE PARTICLE SCATTERING FROM AN IMPURITY

In this section we will analyze the scattering of a single probe atom A from an impurity atom Q. We will formulate the scattering problem, then solve the time-independent and time-dependent Schrödinger equation, to finally obtain the dynamics of wave packets in the lattice.

We consider a probe atom A approaching the impurity from the left, as a plain Bloch-wave with quasimomentum k. Hence the state of the system is given by

$$|k\rangle = \left(\frac{a}{2\pi}\right)^{1/2} \sum_j e^{ikx_j} |j\rangle, \tag{8}$$

where $|j\rangle = |Q\rangle \otimes a_j^\dagger |\text{vac}\rangle$ is the joint state of the atoms A and Q, with A (Q) localized in the lowest vibrational state of the well j (the impurity well $j=0$) and a is the lattice spacing.

The free evolution of the system is given by the hopping of the atoms A between neighboring sites at the tunneling rate J, whereas the composite molecule M is detuned by Δ from the threshold for the joint state of A and Q. Thus, with $E_k = -2J \cos ka$ being the energy of a Bloch wave in the first Bloch band with quasimomentum k, we have

$$\begin{aligned} H_0 &= -J \sum_j (|j+1\rangle\langle j| + \text{H.c.}) + \Delta |M\rangle\langle M| \\ &= \int_{-\pi/a}^{\pi/a} dk E_k |k\rangle\langle k| + \Delta |M\rangle\langle M|, \end{aligned} \tag{9}$$

where $|M\rangle$ denotes the molecular bound state localized on the impurity site. From Eq. (9) we obtain the propagation of the incoming plane wave $|k\rangle$ at group velocity $v_k = \partial E_k/\partial k = 2Ja \sin ka$ in the first Bloch band.

Due to the strong confinement of the particles A and Q in the lattices, their interaction is restricted to the impurity site. There, their bare interaction induces an on-site-shift W for the joint atomic state of A and Q on the impurity ($|0\rangle$). Moreover, the photoassociation lasers effectively couple the latter state to the trapped molecular state ($|M\rangle$) at Rabi frequency Ω, yielding

$$V = W|0\rangle\langle 0| + \Omega(|M\rangle\langle 0| + \text{H.c.}). \tag{10}$$

A. Scattering solution

The scattering of a particle A with energy $E = E_k$ in the first Bloch band by the impurity Q is described by a solution of the Lippmann-Schwinger equation (LSE). The scattering wave function $|\phi_+\rangle$ obeys

$$|\phi_+\rangle = |k\rangle + G_0(E + i0^+) V |\phi_+\rangle, \tag{11}$$

with incident plane wave $|k\rangle$ with quasimomentum k ($0 < k < \pi/a$), and $G_0(z) = 1/(z - H_0)$ the free propagator. Expanding the scattering wave function

$$|\phi_+\rangle = \left(\frac{a}{2\pi}\right)^{1/2} \left[\sum_j \alpha_j |j\rangle + \beta |M\rangle\right] \tag{12}$$

the amplitudes α_j and β satisfy

$$\alpha_j = e^{ikx_j} + \mathcal{G}_j(E_k)(W\alpha_0 + \Omega\beta), \tag{13a}$$

$$\beta = \mathcal{G}_M(E_k)\Omega\alpha_0 \tag{13b}$$

with atomic and molecular propagators

$$\mathcal{G}_j(E) = \langle j|G_0(E+i0^+)|0\rangle \equiv \frac{a}{2\pi}\int_{-\pi/a}^{+\pi/a} dk \frac{e^{ikx_j}}{E - E_k + i0^+} = \frac{e^{ik|x_j|}}{iv_k/a},$$

$$\mathcal{G}_M(E) = \langle M|G_0(E+i0^+)|M\rangle \equiv \frac{1}{E - \Delta + i0^+}. \tag{14}$$

Solving Eqs. (13) we find

$$\alpha_j = e^{ikx_j} + \frac{W_k}{iv_k/a - W_k} e^{ik|x_j|}, \tag{15a}$$

$$\beta = \frac{-i\Omega v_k/a}{\Omega^2 + (E_k - \Delta + i0^+)(W - iv_k/a)} \tag{15b}$$

with effective energy dependent interaction

$$W_k = W + \frac{\Omega^2}{E_k - \Delta + i0^+}, \tag{16}$$

where we read off the transmission and reflection amplitudes

$$t_k = \frac{1}{1 + iaW_k/v_k}, \tag{17a}$$

$$r_k = \frac{-1}{1 - iv_k/aW_k}, \tag{17b}$$

respectively.

Note that the presence of the molecular state introduces an effective energy-dependent interaction W_k. This can be interpreted in terms of an effective atomic scattering length with background scattering length proportional to W and a resonant term, corresponding to an optical Feshbach resonance at energy given by the detuning from the molecular state Δ, and width determined by the Rabi frequency Ω.

The scattering matrix

$$S(E_k) = \begin{pmatrix} r_k & t_k \\ t_k & r_k \end{pmatrix} \tag{18}$$

is unitary, as follows readily from the above expressions (17). This implies $T_k + R_k \equiv |t_k|^2 + |r_k|^2 = 1$. We can assign

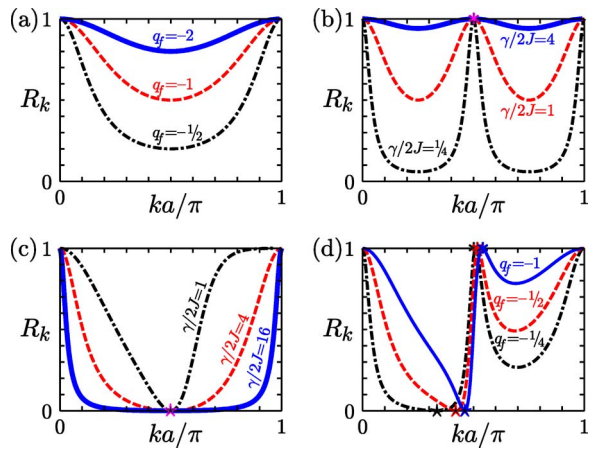

FIG. 5. (Color online) Reflection coefficient R_k, showing in (a) partial reflection for bare background collisions $W\neq 0$ but $\Omega=0$, i.e., $q_f=-1/2,-1,-2$ (dotted, dashed, full line) and $\gamma=E_R=0$, (b) complete reflection at $k_0=\pi/2a$ for $\gamma/2J=1/4,1,4$ (dotted, dashed, full line) and $E_R=q_f=0$, cf. $R\approx 1$ for $\gamma/2J=4$ (full line), (c) perfect transmission at $k_0=\pi/2a$ for $\gamma/2J=1,4,16$ (dotted, dashed, full line), $q_f=-2$ and $E_R=\gamma/4$, cf. $R\approx 0$ for $\gamma/2J=16$ (full line), (d) the asymmetry of the Fano profiles for $q_f=-1/4,-1,-4$ (dotted, dashed, full line), $\gamma/2J=1/2$ and $E_R=0$.

phase shifts $t_k \pm r_k=\exp(i\delta_k^{\pm})$ for the symmetric and antisymmetric states $|k\rangle\pm|-k\rangle$, $\delta_k^{+}=-2\arctan(aW_k/v_k)$ and $\delta_k^{-}=0$, respectively, so that $R_k=\sin^2(\delta_k^{+}/2)$.

B. Discussion of the scattering amplitudes

In the absence of molecular couplings ($\Omega=0$) the on-site interaction W between the B atom and the impurity Q always gives rise to *partial* reflection and transmission, see Fig. 5(a),

$$R_k = 1 - T_k = \frac{W^2}{W^2 + 4J^2\sin^2(ka)} < 1. \tag{19}$$

The significant new feature introduced by the optical Feshbach resonance is that we can achieve essentially complete blocking ($R_k=1$) and complete transmission ($T_k=1$). We obtain this in the limits $\Omega \gg J$ and $\Delta=0$, and $\Omega \gg J$ and $\Delta=-\Omega^2/W$, respectively. Physically, the first case corresponds to tuning to the point of "infinite" scattering length, while the second case corresponds to tuning to the point of "zero" scattering length, respectively.

In the general case the energy dependence of transmission and reflection has the form of a Fano-like profile (see Fig. 5). In the region $|E_k| \ll 2J$ we may neglect the dispersion effects, i.e., $v_k \approx 2Ja$, and obtain Fano line shapes for transmission and reflection as

$$T(\varepsilon) = \frac{1}{1+q_f^2}\frac{(\varepsilon+q_f)^2}{\varepsilon^2+1}, \tag{20a}$$

$$R(\varepsilon) = \frac{1}{1+1/q_f^2}\frac{(\varepsilon-1/q_f)^2}{\varepsilon^2+1}, \tag{20b}$$

where $\varepsilon \equiv (E-E_R)/(\gamma/2)$ is the dimensionless energy in units of the resonance width γ, E_R is the resonance energy and q_f is the Fano q parameter. These parameters of the Fano profile are related to J, W, Δ, Ω by

$$\gamma = \frac{4J\Omega^2}{W^2+4J^2}, \quad \Omega^2 = J\gamma(q_f^2+1), \tag{21a}$$

$$E_R = \Delta - \frac{W\Omega^2}{W^2+4J^2}, \quad \Delta = E_R - \frac{q_f\gamma}{2}, \tag{21b}$$

$$q_f = \frac{-W}{2J}, \quad W = -2Jq_f. \tag{21c}$$

For $W=0$ the asymmetry parameter q_f vanishes, the reflection profile is symmetric, and for $\Omega>0$ resembles a Breit-Wigner-profile, see Fig. 5(b). The maximum $R_k=1$ is attained at $\varepsilon=-q_f$ ($E_k=\Delta$, $|\Delta|<2J$) and has a width $\gamma=\Omega^2/J$.

For finite background collisions $q_f\neq 0$ ($W\neq 0$) the transmission profile is asymmetric, and shows an additional minimum $R_k=0$ at $\varepsilon=-1/q_f$ ($E_k=\Delta-\Omega^2/W=\Delta_\star$, $|\Delta_\star|<2J$), see Fig. 5(c). Near the edges of the Bloch band, $k_\pm=(\pi\mp\pi)/2a$ ($E_k=\pm 2J$), transmission and reflection deviate from the Fano line shape (20). There the group-velocity $v_k\to 0$ and thus also the transmission T_k vanishes, unless the dressed resonance $\Delta_\star$ is tuned to respective edge of the Bloch band. The transmission coefficient are given by

$$T_{k\approx k_\pm} \approx \frac{4J^2a^2(k-k_\pm)^2}{[W-\Omega^2/(\Delta\mp 2J)]^2} \quad \text{for } \Delta_\star \neq \pm 2J,$$

$$T_{k\approx k_\pm} \approx 1 - \frac{W^4a^2(k-k_\pm)^2}{2\Omega^4} \quad \text{for } \Delta_\star = \pm 2J. \tag{22}$$

The reflection coefficient R_k as a function of energy $-2J<E_k<+2J$ is shown in Fig. 5.

In the absence of molecular coupling, $\gamma=0$ ($\Omega=0$), the reflection is unity at the band edges, $k=0$, π/a, and decreases within the Bloch-band due to the increase of the group-velocity [see Fig. 5(a)]. The profile is symmetric about the middle of the Bloch band, $k=\pi/2a$, where it attains its minimum

$$R_k = \frac{1}{1+q_f^{-2}} = \frac{1}{1+(2J/W)^2}.$$

In the presence of molecular couplings, $\gamma\neq 0$ ($\Omega>0$), and for $E_R=q_f=0$ the reflection profile is still symmetric about $k=\pi/2a$ [see Fig. 5(b)]. However, now it approaches its maximum $R_k=1$, at $k=\pi/2a$, and has now two minima at $k\approx\pi/4a$ and $k\approx 3\pi/4a$, given by

$$R_k = \frac{1}{1+(2J/\gamma)^2} = \frac{1}{1+(\sqrt{2}J/\Omega)^4}.$$

For $\gamma, q_f\neq 0$ we obtain an asymmetric Fano profile [see Fig. 5(d)], which for $|E_R+q_f\gamma/2|=|\Delta|<2J$ shows complete reflection $R_k=1$, at $\varepsilon=-q_f$, while for $|E_R-\gamma/2q_f|<2J$ one has perfect transmission $R_k=0$, at $\varepsilon=+1/q_f$. The reflective and transmissive resonance are present regardless of the magnitude of q_f, and their width is $\propto\gamma$. However, for $\gamma\leqslant 8J|q_f+1/q_f|$ they may both occur within the physical

energy range of the Bloch band [see Fig. 5(d)], while for $\gamma > 8J|q_f + 1/q_f|$ only one resonance appears [see Figs. 5(b) and 5(c)]. Thus in the limit $\gamma \gg 8J|q_f + 1/q_f|$ we achieve complete blocking, $R_k = 1$ for all k, by tuning $E_R \approx -q_f\gamma/2$ [see full line in Fig. 5(b)]. Within the same limit we can also efficiently screen any background interaction W and achieve complete transparency, $T_k = 1$ for all k, by tuning $E_R \approx \gamma/2q_f$ [see full line in Fig. 5(c)].

C. Interference mechanism

Physically, the features of complete blocking ($R_k = 0$) and complete transmission ($T_k = 0$) are induced by an interference mechanism, as the probe atom may tunnel via two interfering paths of dressed atomic+molecular states, as depicted in Fig. 4. For simplicity we start by elucidating the underlying interference mechanism (present for $\Omega \neq 0$) in the regime of strong coupling, $\Omega^2 \gg (2J)^2 + |W\Delta|$. In this regime we can consider the local dynamics within the individual sites, and treat the tunneling J by means of perturbation theory.

To zeroth order in J the Hamiltonian H decouples the dynamics of the individual sites j as

$$H^{(0)} = W|0\rangle\langle 0| + \Omega|0\rangle\langle M| + \Omega|M\rangle\langle 0| + \Delta|M\rangle\langle M|. \quad (23)$$

Outside the impurity ($j \neq 0$) its eigenstates are the joint states of the atoms A and Q, $|j\rangle$, with energy $E_0 = 0$, whereas on the impurity ($j = 0$) the strong coupling Ω between the atomic state $|0\rangle$ and the molecular state $|M\rangle$ induces the two states to split into two dressed state $|E_\pm\rangle$ of atoms+molecules with energy $E_\pm$, see Fig. 4. By diagonalizing the 2×2 matrix in Eq. (23) we obtain the amplitudes and energy of the dressed states as

$$|E_\pm\rangle = \left[\frac{1 \pm \xi}{2}\right]^{1/2}|0\rangle \pm \left[\frac{1 \mp \xi}{2}\right]^{1/2}|M\rangle, \quad (24a)$$

$$E_\pm = \frac{W + \Delta}{2} \pm \left[\Omega^2 + \left(\frac{W - \Delta}{2}\right)^2\right]^{1/2}, \quad (24b)$$

$$\xi = \frac{W - \Delta}{[(W - \Delta)^2 + 4\Omega^2]^{1/2}}, \quad (24c)$$

where ξ characterizes the asymmetry of the amplitudes, i.e., for $\xi = 0$ ($W = \Delta$) the dressing is completely symmetric while for $|\xi| = 1$ ($\Omega = 0$) the atomic and molecular state decouple. From Eq. (24b) we see that for $\Omega \gg |W\Delta|$ the dressed states are far off-resonant from $E = 0$, and hence will be only virtually populated.

The effects of the hopping of the atom A on the $E \approx 0$ modes $|j \neq 0\rangle$ can be accounted by means of an effective Hamiltonian H_{eff}. Following Ref. [1] we obtain the dynamics as a perturbative series in the hopping amplitude J, $H_{\text{eff}} = H^{(0)} + H^{(1)} + H^{(2)} + \cdots$. To first order in J one obtains

$$H^{(1)} = -J\sum_{j<0}|j\rangle\langle j-1| - J\sum_{j>0}|j\rangle\langle j+1| + \text{H.c.}$$
$$= \sum_{\alpha=L,R}\int dk E_k |k_\alpha\rangle\langle k_\alpha|, \quad (25)$$

where $|k_L\rangle$ ($|k_R\rangle$) are the Bloch-waves with quasi-momentum k on the left (right) side of the impurity site

$$|k_{L,R}\rangle = \left(\frac{a}{2\pi}\right)^{1/2}\sum_{\pm j>0} e^{+ikx_j}|j\rangle.$$

Thus the flat dispersion relation $E^{(0)} = 0$ on the left and right side of the impurity is bent to $\varepsilon(k) = -2J\cos(ka)$, i.e., we recover the Bloch band(s).

To second order in J we obtain

$$H^{(2)} = -J_{\text{eff}}\sum_{i,j=\pm 1}|i\rangle\langle j|, \quad (26)$$

$$J_{\text{eff}} = \frac{J^2}{2}\left[\frac{1+\xi}{E_0 - E_+} + \frac{1-\xi}{E_0 - E_-}\right] = \frac{J^2\Delta}{\Omega^2 - W\Delta}. \quad (27)$$

We see that tuning on resonance $\Delta = 0$ the two contributions in Eq. (27) cancel each other as

$$J_{\text{eff}} = \frac{J^2}{\sqrt{W^2 + \Omega^2}} - \frac{J^2}{\sqrt{W^2 + \Omega^2}} = 0, \quad (28)$$

which gives perfect blocking by the impurity. Furthermore, from Eq. (24b) we obtain that for $\Delta_\star = \Delta - \Omega^2/W = 0$ one of the dressed states $|E_B\rangle$ becomes a resonance for an incoming particle ($E_B = E_0 = 0$) and for $\Omega \neq 0$ provides for complete transmission by means of photoassisted tunneling. The described interference mechanism induced by the optical Feshbach resonance is in marked contrast to the situation where one has background collisions. There the particle A can tunnel only via one path through the impurity ($|\xi| = 1$), and therefore the effective hopping rate is always finite, i.e., $J_{\text{eff}} = -J^2/W \neq 0$.

D. Discussion of bound states

For completeness we here derive the exact bound-state spectrum of H. For the exact scattering solution, detailed in Sec. III, the bound states take the role of dressed states $|E_\pm\rangle$, which are responsible for the interference mechanism. We will show that for arbitrary Ω there are always *two* bound states, provided $|\Delta - \Omega^2/W| > 2J$. For $|\Delta - \Omega^2/W| \leqslant 2J$ one of the bound states turns into a resonance, which makes the impurity completely transparent for the atom A, $T_k = 1$. Furthermore, we will show that the bound states extends over several lattice sites for $\Omega, W, \Delta \sim J$. This is in marked contrast to the perturbative result, where the dressed states were localized on the impurity site, cf. Eq. (24a).

We obtain the bound states wave functions $|\phi_B\rangle$ from the homogeneous Lippmann-Schwinger equation

$$|\phi_B\rangle = G_0(E)V|\phi_B\rangle, \quad (29)$$

where ϕ_B denotes the bound state with energy $E \equiv E_B$ ($|E_B| > 2J$). Using the ansatz

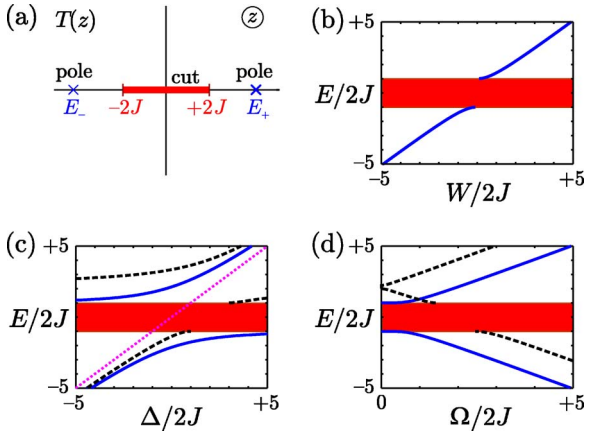

FIG. 6. (Color online) (a) The analytic properties of the T matrix in the complex plane. The cut on the real axis is due to the propagation of (dressed) Bloch waves. The two poles on the real axis correspond to two bound states and give rise to interference. (b)–(d) The spectrum E_n of the Hamiltonian $H=H_0+V$ as a function of (a) the on-site-shift W on the impurity for $\Omega=0$, (b) the detuning Δ for $\Omega/J=2$ and $W=0$ (solid lines), for $\Omega/J=4$ and $W=0$ (dashed lines), for $\Omega/J=2$ and $W/J=4$ (dash-dotted lines), (c) the Rabi-frequency Ω for $\Delta=W=0$ (solid lines), for $\Delta/J=4$ and $W=0$ (dashed lines), for $\Delta/J=W/J=4$ (dash-dotted lines). The continuous (scattering) spectrum, i.e., the Bloch band E_k, is indicated as a shaded region $-2J<E_k<2J$, whereas the bound state(s) E_B are shown as (solid, dashed, dash-dotted) lines.

$$|\phi_B\rangle = \sum_j \alpha_j |j\rangle + \beta |M\rangle \tag{30}$$

we find that the atomic and molecular amplitudes α_j and β satisfy

$$a_j = \mathcal{G}_j(E_B)[W\alpha_0 + \Omega\beta], \tag{31a}$$

$$\beta = \mathcal{G}_M(E_B)\Omega\alpha_0. \tag{31b}$$

The atomic and molecular propagators are given by

$$\mathcal{G}_j(E_B) = \langle j|G_0(E_B)|0\rangle = \frac{e^{-|x_j|/r_B}[\mathrm{sgn}(-E_B)]^j}{-2J\sinh(\kappa_B a)},$$

$$\mathcal{G}_M(E_B) = \langle M|G_0(E_B)|0\rangle = \frac{1}{E_B-\Delta}, \tag{32}$$

and $r_B=a/\mathrm{acosh}(|E_B|/2J)>0$ denotes the size of the bound state.

For convenience we first consider the case $\Omega=0$. There the molecular state decouples from the atomic ones, and we have one bound state $|\phi_1\rangle=|M\rangle$ with energy $E_1=\Delta$. Moreover, for $W\neq 0$ we have another bound state $|\phi_2\rangle$ with energy $E_2=\mathrm{sgn}(W)\sqrt{W^2+(2J)^2}$. Its amplitudes are given by $\beta=0$ and

$$\alpha_j = \left[\tanh\left(\frac{a}{r_B}\right)\right]^{1/2} e^{-|x_j|/r_B}[\mathrm{sgn}(-W)]^j,$$

with the size $r_B=a/\arccos\sqrt{1+(W/2J)^2}$. The spectrum of the system is plotted in Fig. 6(b) as a function W. For attractive (repulsive) interaction $W<0$ $(W>0)$ the energy of the bound state ϕ_2, lies below (above) the Bloch band, i.e., $E_2<-2J$ $(E_2>2J)$, respectively. For $|W|<2J$ bound state ϕ_2 extends over several lattice sites, while for $|W|\gg 2J$ it is localized on the impurity.

In the case $\Omega\neq 0$ a nontrivial solution of Eq. (31) requires

$$-E_B\left[1-\left(\frac{2J}{E_B}\right)^2\right]^{1/2} = W + \frac{\Omega^2}{E_B-\Delta}, \tag{33}$$

which determines the bound-state spectrum $E_B(W,\Delta,\Omega)$. From Eq. (31) we obtain the atomic and molecular amplitudes as

$$\alpha_j = \beta\frac{E_B-\Delta}{\Omega}e^{-|x_j|/r_B}[\mathrm{sgn}(-E_B)]^j, \tag{34a}$$

$$\beta = \left[1+\frac{(E_B-\Delta)^2}{\Omega^2\sqrt{1-\frac{4J^2}{E_B^2}}}\right]^{-1/2}. \tag{34b}$$

We solve Eq. (33) by expressing one of the parameters, either W, Ω, or Δ, in terms of the bound-state energy E_B,

$$\Delta(E_B) = E_B + \frac{\Omega^2}{E_B\sqrt{1-4J^2/E_B^2}+W}, \tag{35a}$$

$$\Omega(E_B) = \left[(\Delta-E_B)\left(E_B\sqrt{1-\frac{4J^2}{E_B^2}}+W\right)\right]^{1/2}, \tag{35b}$$

$$W(E_B) = E_B\sqrt{1+\frac{4J^2}{E_B^2}}+\frac{\Omega^2}{E_B-\Delta}. \tag{35c}$$

Inverting the functions Eq. (35) for E_B yields E_B as a function of Δ, Ω and W, respectively. For fixed Δ, Ω, W we carry out the inversion by plotting in Fig. 6 the right-hand side of Eq. (35a)–(35c) as a function of E_B. In particular in Fig. 6(b) we plot detuning Δ as a function of E_B for constant Ω and W, in Fig. 6(c) we plot Rabi frequency Ω as a function of E_B for constant Δ and W, and in Fig. 6(d) we plot on-site shift W as a function of E_B for constant Δ and Ω. In the following we will give a detailed discussion of Fig. 6.

For no background collisions, $W=0$, and arbitrary detuning Δ, one always has two bound states $\phi_{1,2}$ with energy $E_1<-2J$ and $E_2>2J$, respectively, see solid line in Fig. 6(c) corresponding to $\Omega=4J$. For $|\Delta|\gg\Omega$ the energy one bound-state approaches Δ and is wave function becomes localized on the impurity, while the energy the other approaches the Bloch band and its wave function extends over several lattice sites. For $\Delta=0$ the two bound states are split symmetrically, and their energies are given by [see solid line in Fig. 6(d)]

$$E_{1,2} = \pm\sqrt{2J^2+\sqrt{4J^2+\Omega^2}}. \tag{36}$$

The symmetric splitting allows for complete reflection at $E_k=0$. In the limit $\Omega\gg 2J$ we recover the perturbative result Eq. (24b), as the energies of the bound states approach $E_\pm=\pm\Omega$, with their wavefunctions given by the dressed states $|E_\pm\rangle$, cf. Eq. (24a).

For finite onsite shift, $W\neq 0$, we also have two bound-states provided $|\Delta_\star|\equiv|\Delta-\Omega^2/W|>2J$, see dashed lines in

Figs. 6(c) and 6(d). With increasing detuning Δ the energy of the bound state ϕ_1 approaches the Bloch band from below until crossing it for $-2J+\Omega^2/W<\Delta<+2J+\Omega^2/W$. In this parameter regime there is merely one bound state, while the other develops a resonance. This allows for perfect transparency at $E_k=\Delta-\Omega^2/W$.

Finally we remark that the size r_B of the bound states is inversely proportional to the separation of their energy E_B from their Bloch band. Thus for $|E_B|\ll 2J$ the wave function of the bound states extends over several lattice sites. For $|E_B|\gg 2J$ the bound states are localized on the impurity and we recover the results of the previous section.

E. Wave-packet dynamics

As an illustration of the time dependence of the interference mechanism we simulate the evolution of a Gaussian wave packet $\psi(t)$ with mean quasimomentum $k=\pi/2a$ incident from the left of the impurity. These wave packets are obtained as superposition of the scattering solutions ϕ_+ of Sec. III, i.e., their atomic and molecular amplitudes $\alpha_j(t)=\langle j|\psi(t)\rangle$ and $\beta(t)=\langle M|\psi(t)\rangle$, are obtained as

$$\alpha_j(t)=\sum_{j'} U_{j,j'}(t)\alpha_{j'}(0), \tag{37a}$$

$$\beta(t)=\sum_{j'} U_{M,j'}(t)\alpha_{j'}(0), \tag{37b}$$

with the full propagator for the system given by

$$U_{j',j}(t)=\sum_B \frac{e^{-(|x_{j'}|+|x_j|)/r_B-iE_Bt}\,\mathrm{sgn}(-E_B)^{j'+j}}{\frac{|E_B|}{\sqrt{E_B^2+4J^2}}+\left[\frac{\Omega}{E_B-\Delta}\right]^2}$$
$$+\frac{a}{2\pi}\int dk e^{-iE_kt}[e^{+ik|x_{j'}-x_j|}+r_ke^{+ik(|x_{j'}|+|x_j|)}],$$

$$U_{M,j}(t)=\sum_B \frac{e^{-|x_j|/r_B-iE_Bt}\,\mathrm{sgn}(-E_B)^j}{\sqrt{1+\frac{|E_B|(E_B-\Delta)^2}{\Omega^2\sqrt{E_B^2-4J^2}}}}$$
$$+\frac{a}{2\pi}\int dk e^{-iE_kt}\left[\frac{\Omega t_k}{E_k-\Delta+i0^+}e^{+ik(|x_j|)}\right]. \tag{38}$$

On the left side of Fig. 7 we plot the atomic populations of the individual sites, $n(x_j,t)=|\alpha_j(t)|^2$. The right side shows the corresponding atomic populations of the atom A on the left, $n_L=\Sigma_{j<0}n(x_j,t)$ (dashed line), and on the right side of the impurity, $n_R=\Sigma_{j>0}n(x_j,t)$ (dashed-dotted line). We also plot the population on the impurity, i.e., the atomic population, $n_0=n(x_0,t)$ (solid line), and the molecular population, $n_M(t)=|\langle M|\psi(t)\rangle|^2$ (dotted line). The three different sets in Fig. 7 correspond to different coupling strengths Ω and detunings Δ. For all cases we choose $W=2J$. In Fig. 7(a) we have $\Omega=0$: the atom is partially reflected from the impurity with $R_k=1$. In Fig. 7(b) we set $\Omega=2J$ and $\Delta=0$, which gives rise to complete reflection of the wave packet $R_k=1$. In Fig. 7(c) we have $\Omega=2J$, but now $\Delta=2J$. We have complete transmission of the atom through the impurity, $T_k=1$. All this is consistent with the results of Sec. III.

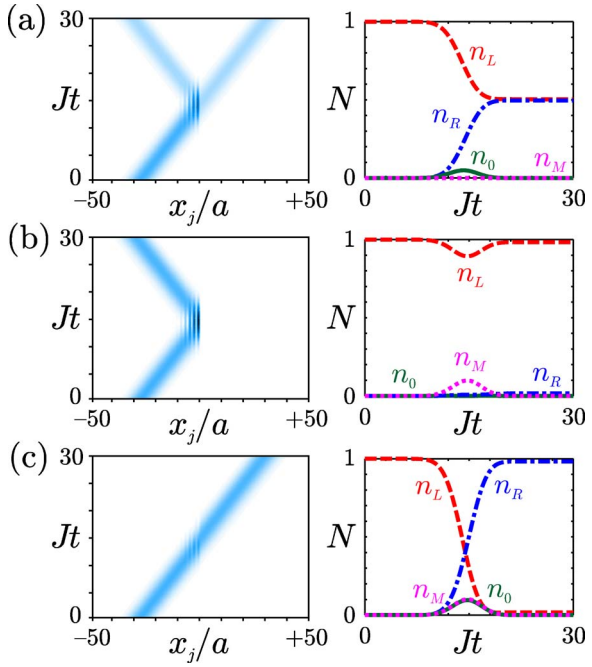

FIG. 7. (Color online) Evolution of a Gaussian wave packet with mean quasimomentum $k=\pi/2a$ for $W=2J$ and (a) $\Omega=0$, (b) $\Omega=2J$, $\Delta=0$, and (c) $\Omega=\Delta=2J$. On the left side the atomic density $n(x_j,t)$ of atoms A is plotted (darker region correspond to higher density). The right side shows the corresponding population of atoms A of the sites to the left $n_L(t)$ (dashed-line), to the right $n_R(t)$ (dashed-dotted line), and on the impurity site $n_0(t)$ (solid line), as well as the population of the molecular state $n_M(t)$ (dotted line).

IV. MANY BODY SCATTERING FROM AN IMPURITY

In this section we will analyze the evolution of a 1D lattice gas of *many* atoms A interacting with an impurity atom Q. Since the statistics of the atoms A plays a dominant role, we will consider the cases of fermionic and bosonic atoms, separately. In this context we will study analytically the limiting cases of an ideal Fermi gas, an ideal Bose gas, and a Tonks gas. An exact numerical treatment of the dynamics for the lattice gas having arbitrary interaction U is given in Ref. [24].

A. Ideal Fermi gas

We first consider the case, where the probe atoms A are spin-polarized fermions. The Hamiltonian for the system is given by

$$H=-J\sum_j (a_j^\dagger a_{j+1}+a_{j+1}^\dagger a_j)+\Delta|M\rangle\langle M|+\Omega(|M\rangle\langle Q|a_0+a_0^\dagger|Q\rangle$$
$$\times\langle M|)+W_Q|Q\rangle\langle Q|a_0^\dagger a_0+W_M|M\rangle\langle M|a_0^\dagger a_0, \tag{39}$$

where the operators $a_j^\dagger$ (a_j) create (annihilate) an atom A on site j, and obey the canonical anticommutation relations

$\{a_i, a_j^\dagger\} = \delta_{ij}$ and $\{a_i, a_j\} = \{a_i^\dagger, a_j^\dagger\} = 0$. Moreover, $|Q\rangle$ ($|M\rangle$) denote the states with an atom Q (a molecule in state M) on the impurity, and W_Q (W_M) is the onsite shift for an atom A and an atom Q (a molecule M) on the impurity.

For simplicity henceforth we will restrict ourselves to the case of equal on-site shifts $W_M = W_Q \equiv W$. In this case we may rewrite the Hamiltonian as

$$H = -J\sum_j (a_j^\dagger a_{j+1} + a_{j+1}^\dagger a_j) + W a_0^\dagger a_0 + \Delta f^\dagger f + \Omega(f^\dagger a_0 + a_0^\dagger f), \tag{40}$$

where the ladder operators $f^\dagger \equiv |M\rangle\langle Q|$ and $f \equiv |Q\rangle\langle M|$ obey standard fermionic anti-commutation relations and anticommute with a_j and $a_j^\dagger$. The corresponding equations of motions for a_j and f are linear, provided $W_M = W_Q$. Thus for a Fermi gas of N atoms A the scattering off the impurity atom Q will occur independently for each fermion a_k with scattering amplitudes t_k and r_k, according to their quasimomentum k, see Eq. (17). The details of this calculation will be given below.

We will here detail the time-dependent scattering for a Fermi gas of N atoms A. For concreteness we assume the fermions to be initially trapped in a box of M sites to the left the impurity atom Q. The corresponding wave function of the system is given by

$$|\Psi(t=0)\rangle = \prod_{n=1}^{N}\left[\sum_j \alpha_j(k_n) a_j^\dagger\right]|Q\rangle,$$

$$\alpha_j(k_n) = \sqrt{\frac{2}{M+1}}\begin{cases}\sin(k_n x_j) & \text{for } -M \leqslant j \leqslant -1,\\ 0 & \text{else,}\end{cases} \tag{41}$$

where the quasimomenta $k_n = n\pi/(M+1)a$. This corresponds to a Fermi sea filled from $E_0 = -2J$ up to $E_F = 2J\cos(k_F a)$, where $k_F = N\pi/a(M+1)$ is the Fermi momentum, which is proportional to the initial filling factor $\nu = N/M$.

At time $t=0$ we open the impurity [see Fig. 1(b)], and from Eq. (40) we obtain the evolution of the system as

$$|\Psi(t)\rangle = \prod_{n=1}^{N}\left[\sum_j \alpha_j(k_n,t) a_j^\dagger + \beta(k_n,t) f^\dagger\right]|Q\rangle, \tag{42a}$$

$$\alpha_j(k_n,t) = \sum_{j'} U_{j,j'}(t)\alpha_{j'}(k_n), \tag{42b}$$

$$\beta(k_n,t) = \sum_{j'} U_{M,j'}(t)\alpha_{j'}(k_n), \tag{42c}$$

where $U_{\alpha,j}(t)$ are the single-particle propagators, cf. Eq. (38). According to Eq. (42a) the scattering from the impurity occurs independently for each particle in the initial Fermi sea, with scattering amplitudes t_k and r_k given in Eq. (17) for $0 < k \leqslant k_F$. The atomic and molecular densities are thus given by the sum of the probabilities for the single fermions in the Fermi gas

$$n(x_j,t) = \langle a_j^\dagger a_j\rangle_t = \sum_{n=1}^{N} |\alpha_j(k_n,t)|^2, \tag{43a}$$

$$n_M(t) = 1 - n_Q(t) = \sum_{n=1}^{N} |\beta(k_n,t)|^2. \tag{43b}$$

Opening the switch allows the system to dynamically expand to the right on as an semi-infinite system out of equilibrium. To characterize the quasimomentum distribution of the semi-infinite system the discrete quantum numbers for the quasimomenta k_n of the box are no longer good. Their role are taken by a continuum of quasimomenta $-\pi/a < k \leqslant \pi/a$ and the corresponding atomic quasimomentum distribution is given by

$$n(k,t) = \frac{a}{2\pi}\sum_{j,j'} e^{-ik(x_{j'}-x_j)}\langle a_{j'}^\dagger a_j\rangle_t$$

$$= \frac{a}{2\pi}\sum_{n=1}^{N}\left|\sum_j e^{-ikx_j}\alpha_j(k_n,t)\right|^2.$$

The initial quasimomentum distribution is given by a step function, which is smoothed around k_F due to the finite size of the initial box trapping M, i.e.,

$$n(k,0) = \frac{a}{2\pi}\sum_{n=1}^{N}\frac{\sin^2(k_n a)}{M+1}\frac{1-(-1)^n\cos[ka(M+1)]}{[\cos(k_n a)-\cos(ka)]^2}$$

$$\approx \frac{a}{2\pi}\sum_{n=1}^{N}\frac{M+1}{2}\sum_{\pm}\mathrm{sinc}^2\left[(ka \pm k_n a)\frac{M+1}{2}\right]. \tag{44}$$

and corresponds to a system out of equilibrium. Therefore there are also fermions present in the system with $k > k_F$. However, in the limit of a large box and large particles numbers, $M \geqslant N \gg 1$, the fraction of fermions with quasimomenta larger that the fermi momentum vanishes as $\delta n = \int_{|k|>k_F} n(k,0)/N \propto 1/M$. In this limit one recovers the sharp form of step function $n(k,0) \approx (M+1)(a/\pi)\theta(k_F a - |k|a)$.

In Figs. 8(a)–8(c) we show the evolution for a Fermi-sea with $\nu = 0.76$, i.e., $N = 38$ particles initially on $M = 50$ sites. For each simulation we have $W = \Delta = 0$, but the driving varies as $\Omega/J = 0, 1, 2$ in Figs. 8(a)–8(c), respectively. On the left side we plot the atomic density $n(x_j,t)$ (darker regions correspond to higher density). To the right we plot the respective momentum profiles $n(k,t)$ for the Fermi gas at times $t = 0, M/2J, M/J$ (from bottom to top). This times are indicated by arrows for each figure.

In Fig. 8(a) we see the evolution of the noninteracting system, $\Omega = 0$. The atomic cloud expands freely to the right after opening the switch at $t=0$. The corresponding momentum distribution is initially given smooth step-function, see Eq. (44), where the fraction of fermions with $|k| > k_F$ is $\delta n \approx 0.0244$ (see profile in bottom inset). With progressing time the gas is forward scattered, i.e., its mean quasimomentum becomes $k > 0$, as fermions with $k < 0$ get reflected onto $k' = -k > 0$ by the hard wall at $x_j = -(M+1)a$, while those modes with $k > 0$ can freely expand through the switch. The

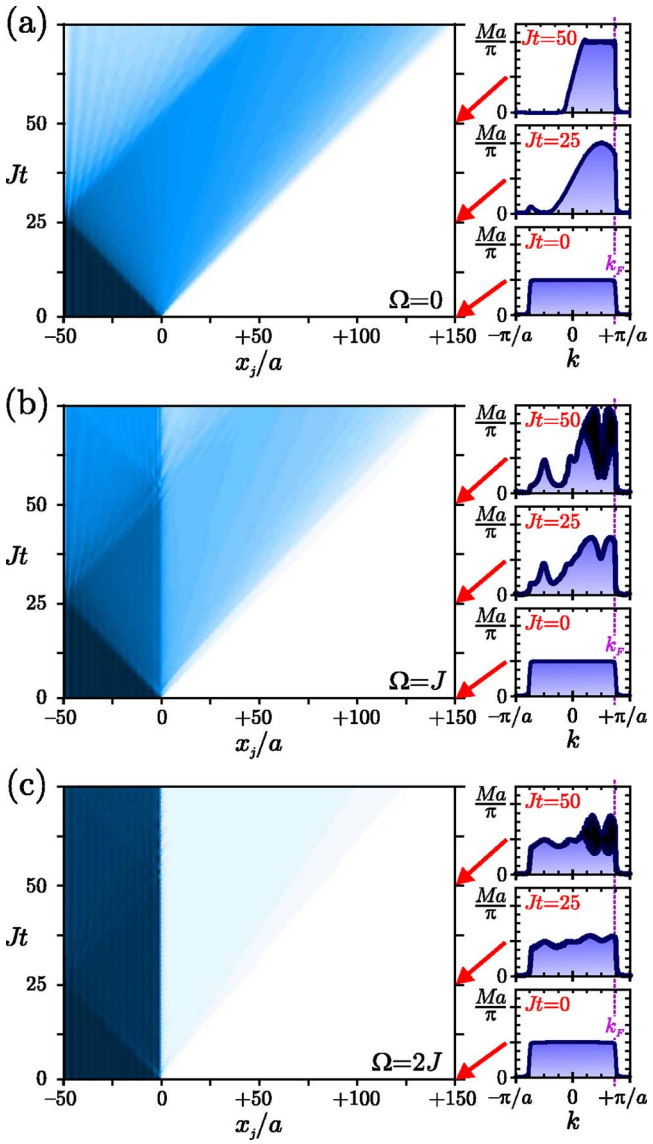

FIG. 8. (Color online) Evolution of a Fermi gas with filling factor $\nu=0.76$ ($N=38$ particles on $M=50$ sites) after opening the switch at $t=0$. The effective Rabi frequency is (a) $\Omega=0$, (b) $\Omega=J$ (c) $\Omega=2J$, and in all three cases we have $W=\Delta=0$. The left side shows the atomic density $n(x,t)$ (darker regions correspond to higher density), and the right side the momentum distribution $n(k,t)$ at time $t=0,M/2J,M/J$ (from bottom to top). The corresponding density distribution at this three times are indicated by arrow. The black regions in the inset for $t=M/J$ near $k\approx\pi/2a$ correspond to interference fringes with period $\delta k=2\pi/(M+1)$ (not resolved in the figure) between fermions which directly passed the impurity and those which passed the impurity only after being reflected once.

modes with $k=-\pi/2a$ have the largest group velocity v_k and therefore get scattered first from the left wall of the semi-infinite system. This induced an enhancement of the population of modes near $k=\pi/2a$ with progressing time and results into an broad asymmetric quasimomentum profile centered about mean quasimomentum $k=+\pi/2a$ (see profile in middle inset). For large times $t\gg M/2J$ the quasimomentum distribution becomes very asymmetric toward $k>0$ as all the fermions with $k<0$ (except those with a very small v_k

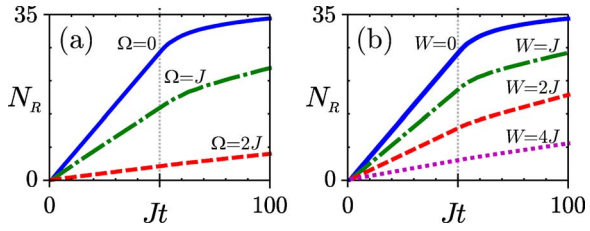

FIG. 9. (Color online) The number of atoms A transmitted through the impurity as a function of time t, $N_R(t)$, for a Fermi gas with $\nu=0.76$. (a) We have $\Delta=W=0$ and the coupling is $\Omega=0$ (solid line), $\Omega=J$ (dashed-dotted line), $\Omega=2J$ (dashed line). In (b) there is no coupling, $\Omega=0$, but the background interaction are $W=0,J,2J,4J$ (solid, dash-dotted, dashed, dotted line). The system establishes a constant particle current up to $t\approx 50/J$ $\Delta=W=0$ and the coupling is $\Omega=0$ (solid line), $\Omega=M/J=50/J$, and saturates until all $N=38$ atoms A passed the impurity.

near $k=0$ and $k=\pi/a$) where reflected onto $-k>0$ (see profile at top inset).

In Fig. 8(b) we show the behavior for weak laser driving, $\Omega=J$. We notice that there is already substantial blocking by the impurity. The corresponding momentum profiles show that the blocking is mainly due to the complete reflection of fermions with quasimomentum near $k=\pi/2a$ to $k'=-\pi/2a$ (see profile in the middle). For large times $t\sim M/J$ multiple reflections by the impurity and the left side wall occurred for the fastest modes, i.e., those near $k=\pi/2a$. This produces interference fringes for the quasimomentum distribution (see profile in the top).

In Fig. 8(c) we plot the densities for resonant driving with $\Omega=2J$. The transport through the impurity is efficiently blocked by the impurity atom, as the initial densities $n(x_j,t=0)$ and $n(k,t=0)$ are almost completely preserved.

In the following we will consider the number of particles on the right side of the impurity

$$N_R(t)=\sum_{j>0} n(x_j,t), \tag{45}$$

and the corresponding particle current through the impurity I_R:

$$I_R(t)=\frac{dN_R}{dt}(t). \tag{46}$$

They characterize the behavior of the switch.

In Fig. 9(a) we show the number of particles $N_R(t)$, for the same parameters as in Fig. 8, i.e., for each the initial filling factor $\nu=0.76$ and $W=\Delta=0$. The solid line shows N_R for the no coupling to the impurity $\Omega=0$ and corresponds to the densities shown in Fig. 8(a). The dashed-dotted line shows the behavior for $\Omega=J$, see Fig. 8(b), and the dashed line corresponds to $\Omega=2J$, i.e., Fig. 8(c). Moreover, in Fig. 9(b) we show the number of particles $N_R(t)$, for initial filling factor $\nu=0.76$ and $\Omega=\Delta=0$, but for an onsite shift $W=0,J,2J,4J$ (see solid, dash-dotted, dashed, dotted line), respectively. In general, after a short transient period, of the order of the inverse tunneling rate $1/J$, the number of particles on the right side of the impurity increases linearly with

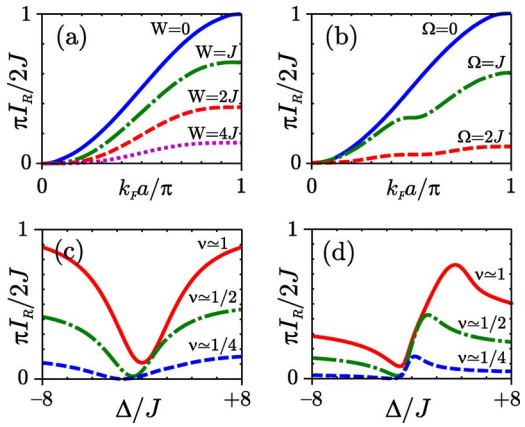

FIG. 10. (Color online) The quasisteady state atomic current I_R through the impurity. Its dependence on the Fermi momentum k_F (corresponding to $\nu \approx k_F a/\pi$) is shown in (a) for $\Omega=0$ but $W=0,J,2J,4J$, and in (b) for $W=\Delta=0$ but $\Omega=0,J,2J$. The dependence of I_R on the detuning Δ is shown in (c) for $\Omega=2J$, $W=0$ and in (d) for $\Omega=W=2J$. The respective filling factor $\nu \approx k_F a/\pi = 1/4, 1/2, 1$ is for each curves is given in the figure.

t. Thereby the system establishes a roughly constant flux of particles I_R through the impurity. The flux persists up to $t \approx M/J$, which is indicated by a vertical dotted line in Figs. 9(a) and 9(b). Then the population on the left side of the impurity is substantially depleted and therefore $N_R(t)$ saturates until all particles tunneled through the impurity, yielding $N_R(t)=N$ and $I_R(t)=0$ for $t \to \infty$.

We are interested in the linear regime. From Eq. (43a) we obtain the constant average current as (see the Landauer formula)

$$I_R = \frac{dN_R}{dt} = \frac{1}{2\pi}\int_0^{k_F} dk v_k T_k, \tag{47}$$

where $v_k = 2Ja\sin(ka)$ is the group velocity of the quasiparticles with quasimomentum k, $k_F = N\pi/(M+1)a$ the Fermi momentum, and T_k the corresponding transmission coefficients, see Eq. (17). Thus the average current is obtained by integrating the Fano profiles $T_k = 1 - R_k$, see, e.g., Fig. 5, up to the Fermi momentum.

For an uncoupled impurity, $W=\Omega=0$, we have $T_k=1$. Thus the current is given up to a constant by the Fermi energy

$$I_R^{(0)} = \frac{E_F + 2J}{2\pi} = \frac{2J}{\pi}\sin^2\left(\frac{N\pi}{2(M+1)}\right). \tag{48}$$

In Fig. 10(b) we plot the dependence of $I_R^{(0)}$ as a function of the Fermi momentum k_F, which correspond to the filling factor $\nu \approx k_F a/\pi$, as a solid line.

For a finite on-site shift $|W|>0$, but no laser-driving $\Omega=0$, we have $T_k<1$, see Eq. (19) and Fig. 5(a). Thus the current through the switch decreases as

$$I_R^{(W)} = \frac{E_F + 2J}{2\pi} - \frac{W^2}{2\pi E_0}\,\mathrm{arccoth}\left(\frac{E_0^2 + 2JE_F}{E_0(E_F+2J)}\right), \tag{49}$$

where $E_0 = \sqrt{W^2+4J^2}$ is the modulus of the bound-state energy. The exponential decay of $I_R^{(W)}$ with increasing coupling strength W, i.e., the arccoth term in Eq. (49), is characteristic for a system with one bound state. The dependence of the current $I_R^{(W)}$ on the Fermi momentum k_F (i.e., on the filling factor ν) is shown in Fig. 10(a). The solid line shows the noninteracting value, $W=0$, while the dash-dotted, dashed, dotted line correspond to $W=J,2J,4J$, respectively.

However, for resonant driving at $\Omega>0$ and couplings $W=\Delta=0$ we obtain a symmetric Fano profile for R_k with respect to $k=\pi/2a$, see Fig. 5(b). Therefore, by integrating the latter profiles we obtain the current as

$$I_R^{(\Omega)} = \frac{E_F + 2J}{2\pi} - \frac{\Omega^2 E_-}{2\pi\sqrt{\Omega^4+4J^4}}\,\mathrm{arccoth}\left(\frac{E_+^2 + 2JE_F}{E_+(E_F+2J)}\right) - \frac{\Omega^2 E_+}{2\pi\sqrt{\Omega^4+4J^4}}\,\mathrm{arccot}\left(\frac{E_-^2 - 2JE_F}{E_-(E_F+2J)}\right), \tag{50}$$

with $E_\pm = \sqrt{\sqrt{\Omega^4+4J^4} \pm 2J^2}$. The arccoth term in Eq. (50) gives the mean effect of the reflection as that typical of a system with one bound-state, while the oscillating arccot term is induced by the presence of two interfering poles in the scattering matrix. The current Eq. (50) is plotted in Fig. 10(b) as a function of the Fermi-momentum k_F for the uncoupled impurity $\Omega=0$ (solid line), for $\Omega=J$ (dashed-dotted line), and for $\Omega=2J$ (dashed line). For finite driving the current $I_R^{(\Omega)}$ shows a plateau at $\nu=1/2$, as all the Bloch waves near $k=\pi/2a$ are completely reflected from the impurity [see Fig. 5(b)]. From Eq. (50) we obtain that already for $\Omega \sim 4J$ the current of particles through the impurity is completely suppressed for arbitrary filling ν, i.e., up to Fermi energy $E_F=2J$.

In the following we discuss the dependence of the current for $\Omega>0$ on the detuning Δ. In Fig. 10(c) we show the current I_R for $\Omega=2J$ but still $W=0$ as a function of the detuning Δ for several initial densities ν. The solid line corresponds to commensurate initial filling, $\nu=1$, the dash-dotted line to half filling, $\nu=1/2$, and the dotted line to a dilute Fermi gas with $\nu=1/4$. The current shows a symmetric profile with a minimum at $\Delta \approx -2J\cos^3(\nu\pi/2)$ and approaches its threshold value $I_R^{(0)}$ for $|\Delta| \gg \Omega$. Notice that the resonance for the many-body Fermi gas with increasing density from the bottom of the Bloch band $\Delta \approx -2J$ toward the middle of the band $\Delta=0$.

For finite $W=2J$ [see Fig. 10(d)] the dependence shows an asymmetric profile and reaches its threshold value $I_R^{(W)}$ [see Eq. (49)] for large detuning, $|\Delta| \gg \Omega^2/|W|$. We notice that although the single fermions in the Fermi sea scatter independently, we obtain a finite current for $\Omega<J$, even on resonance. This is caused by the fact that the various fermionic modes a_k see the resonance a different (energy-dependent) detuning $\Delta - E_k$, which leads to a shift of the minimum (and maximum) of the transmitted current proportional to the density of the Fermi gas, see Figs. 10(c) and 10(d). However, in

the limit of strong driving $\Omega \gg J$ we recover the features of perfect blocking for $\Delta \approx 0$ and of perfect transmission for $\Delta \approx \Omega^2/W$.

B. Ideal Bose gas

We now consider the case, where the probe atoms A are spin-less noninteracting bosons. The Hamiltonian for the system is given by

$$H = -J\sum_j (a_j^\dagger a_{j+1} + \text{H.c.}) + \Delta|M\rangle\langle M| + W_Q|Q\rangle\langle Q|a_0^\dagger a_0 + W_M|M\rangle\langle M|a_0^\dagger a_0 + \Omega(|M\rangle\langle Q|a_0 + a_0^\dagger|Q\rangle\langle M|), \quad (51)$$

where the operators $a_j^\dagger$ (a_j) create (annihilate) an atom A on site j, and obey the canonical commutation relations $[a_i, a_j^\dagger] = \delta_{ij}$ and $[a_i, a_j] = [a_i^\dagger, a_j^\dagger] = 0$. Moreover, $|Q\rangle$ ($|M\rangle$) denote the states with an atom Q (a molecule in state M) on the impurity, and W_Q (W_M) is the onsite shift for an atom A and an atom Q (a molecule M) on the impurity. As in the previous section we will henceforth restrict ourselves to the case of equal on-site shifts $W_M = W_Q \equiv W$. In this case we may rewrite the Hamiltonian as

$$H = -J\sum_j (a_j^\dagger a_{j+1} + a_{j+1}^\dagger a_j) + Wa_0^\dagger a_0 + \Delta\sigma^+\sigma^- + \Omega(\sigma^+ a_0 + a_0^\dagger \sigma^-), \quad (52)$$

where the pauli operators $\sigma^+ \equiv |M\rangle\langle Q|$ and $\sigma^- \equiv |Q\rangle\langle M|$ obey canonical anticommutation relations and commute with a_j and $a_j^\dagger$. The Hamiltonian (52) corresponds a multimode Jaynes-Cummings model.

In the following we will consider the scattering of a gaussian wavepacket of N bosons A, all initially occupying the same single particle state, $\alpha(x_j, t=0)$, approaching the impurity atom Q with mean quasimomentum $\pi/a > k_0 > 0$ and width $\delta k_0 \ll \pi/a$. The corresponding wave function for the system is given by

$$|\Psi(t=0)\rangle = |Q\rangle \frac{1}{\sqrt{N!}}\left[\sum_j \alpha(x_j, t=0) a_j^\dagger\right]^N |\text{vac}\rangle, \quad (53)$$

$$\alpha_0(x_j, 0) = \mathcal{N} e^{-\delta k_0^2 [x_j - x(0)] + ik_0 x_j}, \quad (54)$$

where for $\delta k_0 \ll \pi/a$ the normalization is given by $\mathcal{N}^2 = (2\delta k_0^2 a^2/\pi)^{1/2} = n_0/N$ in terms of the peak density of the Gaussian wave packet $n_0 \equiv n[x(0), t=0]$, and $x(0) \ll 0$ denotes the mean position of the particles A at $t=0$.

For $\Omega = 0$ the equations of motion for a_j decouple from σ^-. Therefore, we obtain the scattering of the bosons A by the impurity, as

$$|\Psi(t)\rangle = |Q\rangle \frac{1}{\sqrt{N!}}\left[\sum_j \alpha(x_j, t) a_j^\dagger\right]^N |\text{vac}\rangle, \quad (55)$$

where the single-particle wave function for finite W was already obtained in Sec. III. For this case all the results obtained in Sec. III hold, and we obtain, e.g., the density as N times the single particle result $n(x_j, t) = N|\alpha(x_j, t)|^2$.

1. Linearization of the impurity

For $\Omega \gg J \gg |\Delta|, |W|$, we obtained in Sec. III that the population of the molecular state was strongly suppressed, i.e., as $(J/\Omega)^2$, and thus we approximate $\sigma^z \to -1$. Thus we linearize the spin, i.e., set $\sigma^+ \to b^\dagger$ and $\sigma^- \to b$, where b and $b^\dagger$ obey canonical commutation relations. The scattering of the bosons A by the impurity is given by

$$|\Psi(t)\rangle \approx \frac{1}{\sqrt{N!}}\left[\sum_j \alpha_j(t) a_j^\dagger + \beta(t) b^\dagger\right]^N |\text{vac}\rangle_A, \quad (56)$$

where the single-particle wave function $\alpha_j(t)$ and the amplitude $\beta(t)$ of the molecular state $b^\dagger|\text{vac}\rangle \equiv \sigma^+|Q\rangle = |M\rangle$, were obtained in Sec. III [see Eq. (38)].

Self-consistency of the replacement $\sigma_z \to -1$ requires that the obtained molecular population $n_m(t) \ll 1$. From the linearization we obtain the molecular population as (see Appendix A)

$$n_m(t) = \frac{n_0}{4\delta k_0^2 \pi}\left|\int dk \frac{\Omega t_k e^{-iE_k t}}{E_k - \Delta} e^{-\tilde{k}^2/4\delta k_0^2 - i\tilde{k}x(0)}\right|^2, \quad (57)$$

where $\tilde{k} \equiv k - k_0$, and the Fourier integral is obtained analytically, e.g., by using a saddle-point method, see Appendix A. We find that the maximal attained molecular population $n_m^\star$ is proportional to the initial density n_0 of the gas. In the case of a broad resonance $\Omega > \delta k_0$ we find

$$n_m^* \approx \frac{n_0 \Omega^2 v_0^2/a^2}{(E_0 - \Delta)^2 v_0^2/a^2 + [\Omega^2 + W(E_0 - \Delta)^2]^2}, \quad (58)$$

with $E_0 = -2J\cos(k_0 a)$ and $v_0 = 2J\sin(k_0 a)$. Moreover, for a extremely narrow resonance, $\Omega < \delta k_0$ and $|\Delta| < J$, one obtains

$$n_m^* \approx \frac{n_0}{2\delta k_0^2 a} \frac{\Omega^2}{W^2 + v_\star^2/a^2} e^{-(k_0 - k_\star)^2/2\delta k_0^2}, \quad (59)$$

where $v_\star = 2Ja\sin(k_\star a)$ and $k_\star \approx \arccos(-\Delta/2J)/a$ denotes the position of the maximum of $T_k/(E_k - \Delta)^2$.

In Fig. 11(a) we show the molecular population, n_m, as obtained by the replacement $\sigma_z \to -1$. In Fig. 11(a) we plot $n_m(t)/n_0$ for an incoming Gaussian wave packet with $k_0 = \pi/2a$ and $\delta k_0 = 0.01\pi/a$ for driving $\Omega = J/4$ (dashed line), $\Omega = J/2$ (dashed-dotted line) and $\Omega = J$ (solid line). In all three cases we have $\Delta = W = 0$. We see that with increasing Rabi frequency Ω the attained molecular population quickly drops as $\sim J^2/\Omega^2$, and that the molecular population closely resembles the density distribution $n(x_j, t=0)$ of the atomic cloud A. In Fig. 11(b) we plot the maximal attained population, n_m^*, as a function of the incoming momentum of the gas, k_0, for $\Omega = J$ and $W = \Delta = 0$. The four lines correspond to different width δk_0 of the wave packet, i.e., $\delta k_0 = 0.001\pi/a$ (solid line), $\delta k_0 = 0.01\pi/a$ (dashed line), $\delta k_0 = 0.1\pi/a$ (dash-dotted line), and $\delta k_0 = 0.2\pi/a$ (dashed line). For a given width δk_0 the molecular population attains its maximum for $k_0 = \pi/2a$, i.e., where we have complete reflection of the wave packet [see Fig. 5(b)]. At the point of complete reflection, $k_0 = \pi/2a$ the population attains its overall maximum for a narrow momentum distribution, i.e., for $\delta k_0 \to 0$ we

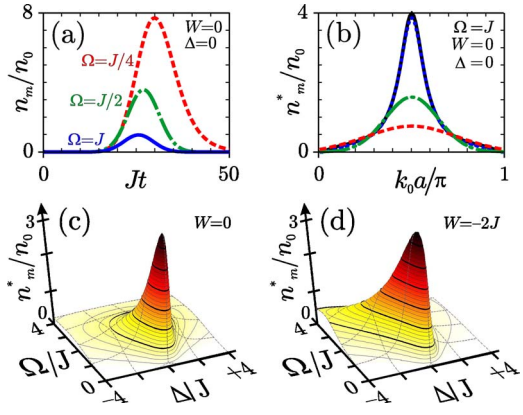

FIG. 11. (Color online) Scattering of a Gaussian wave packet of bosonic atoms B with mean quasimomentum k_0 and width δk_0 as obtained by linearizing the impurity (see text). (a) Molecular population as a function of time for a narrow wavepacket with $k=\pi/a$ and $\delta k_0=\pi/100a$ for $\Omega=J, J/2, J/4$ (solid, dash-dotted, dashed line). (a) The maximal attained molecular population $n_m^\star$ during the interaction process with a weakly coupled impurity ($\Omega=J$, $\Delta=W=0$), as a function of the quasimomentum k_0 of the incoming wave packet. The three lines correspond a wave packet with width $\delta k_0=\pi/200a, \pi/50a, \pi/20a$ (solid, dash-dotted, and dashed line). The dependence of $n_m^\star$ on the parameters Ω and Δ for $k=\pi/2a$ and $\delta k_0=\pi/50a$ in (c) without the presence of background collisions, $W=0$, and in (d) for an onsite shift $W=2J$.

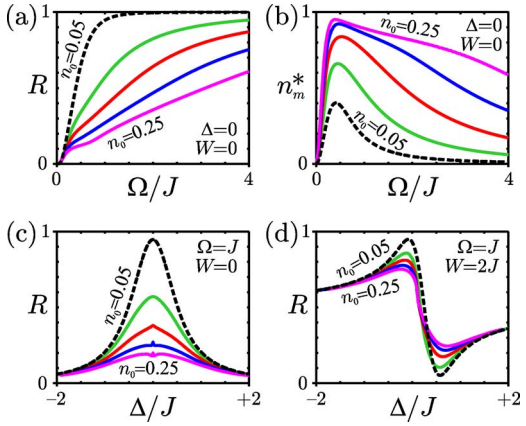

FIG. 12. (Color online) Evolution of a Gaussian wave packet with mean quasimomentum $k=\pi/2a$ and width $\delta k_0=0.02\pi/a$ obtained from the variational ansatz (60). In (a) the reflection coefficient R is plotted as a function of the Rabi frequency Ω for $\Delta=W=0$, and (b) shows the corresponding attained maximal molecular population $n_m^\star$ during the interaction with the impurity atom. The reflection coefficient as a function of the detuning Δ for $\Omega=J$ and (c) $W=0$ and (d) $W=2J$. The various solid lines correspond to initial densities $n_0=0.1, 0.15, 0.20, 0.25$. The dotted line is for $n_0=0.05$ and corresponds to a linearization of the impurity, see Eq. (56).

have $n_m \approx 4n_0$ for $\Omega=J$ and $\Delta=W=0$. The dependence of $n_m^\star$ on the detuning Δ and the Rabi-frequency Ω is shown in Figs. 11(c) and 11(d) for $W=0$ and $W=-2J$, respectively. In both figures the Gaussian wave packet has $k_0=\pi/2a$ and $\delta k_0=0.02\pi/a$, i.e., initially extends about $\sim \pi/a\,\delta k_0=50$ lattice sites. For $W=0$ we have complete reflection of the wave packet for $\Delta=0$, and the attained molecular population is maximal, $n_m \approx 3n_0$, for $\Omega \approx 2J$ and $\Delta \approx 0$ [see Fig. 11(c)]. However, for finite $W=-2J$ we have also complete transmission of the wave packet, i.e., for $\Delta=\Omega/W$. From Fig. 11(d) we notice that for a given Ω the maximal population is shifted from $\Delta \approx 0$ towards the point, where one has complete transmission of the wave packet, i.e., $\Delta \approx \Omega/W$. However, the overall maximum of $n_m^\star$ in both cases, $W=0$ and $W=-2J$, is attained for $\Omega \approx 2J$ and for stronger driving quickly drops as $n_m^\star \approx n_0(2J/\Omega)^2$. As the replacement $\sigma^- \to b$ is self-consistent for a dilute gas with densities $n_0 \ll (n_m^\star/n_0)^{-1}$, we see from Fig. 11 that the approximation holds, even on resonance $\Delta=0$, for strong driving $\Omega > 4J$ up to densities as high as $n_0 \sim 5$ and for small densities $n_0 < 1$ only fails for $\Delta \approx 0$ and $\Omega \approx 2J$.

2. Time-dependent variational ansatz

In the following we use a time-dependent variational ansatz to describe the behavior of the many-body wave function in near resonance $\Delta \approx 0$ for $\Omega \sim J$, i.e. in the regime where the approximation $\sigma_z \to -1$ fails already for small densities, $n_0 > 0.05$. As a generalization of Eq. (30) for $N \geqslant 1$ bosonic atoms A we choose as an number-conserving ansatz for the state of the system

$$|\Psi(t)\rangle = c_Q(t)|Q\rangle \frac{[a_Q(t)^\dagger]^N}{\sqrt{N!}}|\mathrm{vac}\rangle + c_M(t)|M\rangle \frac{[a_M(t)^\dagger]^{N-1}}{\sqrt{(N-1)!}}|\mathrm{vac}\rangle, \tag{60}$$

where $a_\sigma(t)^\dagger = \Sigma_j \alpha_{j,\sigma}(t) a_j^\dagger$ represent two non-orthogonal time-dependent modes for the field of the bosonic atoms A given that the impurity is in state $\sigma=Q,M$, and the amplitudes for the impurity $c_\sigma(t)$ and for the bosonic wave packets $\alpha_{j,\sigma}(t)$ are normalized as $\Sigma_\sigma |c_\sigma(t)|^2 = \Sigma_j |\alpha_{j,\sigma}(t)|^2$. The equation of motion for variational parameters $c_\sigma(t)$ and $\alpha_{j,\sigma}(t)$, are obtained by minimizing the corresponding action (see Appendix B)

$$S(t) = \frac{\langle \dot{\Psi}_t|\Psi_t\rangle - \langle \Psi_t|\dot{\Psi}_t\rangle}{2i} - \langle \Psi_t|H|\Psi_t\rangle \tag{61}$$

with respect to $c_\sigma(t)^*$ and $\alpha_{j,\sigma}(t)^*$, as a set of coupled nonlinear differential equations, which we integrate numerically. Thus we obtain the dynamics of the system.

In Fig. 12 we show the obtained reflection coefficient

$$R = \lim_{t\to\infty} \frac{1}{N} \sum_{j<0} n(x_j,t) \tag{62}$$

and the attained peak molecular population $n_m^\star$ for a Gaussian wave packet with narrow momentum $k_0=\pi/2a$, i.e., $\delta k_0 = 0.02\pi/a \ll \pi/a$ for initial density $n_0=0.05$, $0.1, 0.15, 0.20, 0.25$ (values indicated in plots). In Fig. 12(a) [Fig. 12(b)] we plot R ($n_m^\star$) as a function of the Rabi frequency Ω for $\Delta=W=0$, i.e., when complete reflection of the wave packet was predicted by the bosonic approximation of the spin. The reflection shows a nonlinear behavior in the density for $\Omega > 0.1$, i.e., decreases as $\sim 1/n_0$ with increasing density n_0. While for $n_0=0.05$ (see dotted line) we have com-

plete reflection of the wave packet for $\Omega > 2J$, for higher densities we still have a finite transmission at $\Omega = 2J$. From Fig. 12(a) we see that with increasing density the transmission coefficient rapidly deviates from the low(zero)-density result and approaches a linear behavior in Ω already for $n_0 = 1/4$. In Fig. 12(a) we plot the dependence of $n_m^\star$ on Ω, which shows that the maximal population is attained for $\Omega \approx J/2$ and decreases as $\sim (J/\Omega)^2$ for $\Omega \gg J n_0$. Moreover, we see that with increasing density, $n_0 > 0.10$, the peak in the molecular population $n_m^\star$ is no longer linear in the density as was predicted by linearization, cf. Eq. (58) and cf. Eq. (58), but saturates toward the unitary limit $n_m^\star \approx 1$. The dependence of the reflection coefficient R on the detuning Δ is plotted in Fig. 12(c) for $\Omega = J$ and $W = 0$ and in Fig. 12(d) for $\Omega = J$ and $W = 2J$. In the limit of a very dilute Bose-gas (see dashed lines for $n_0 = 0.05$) we obtain the single-particle result $T = |t(k_0)|^2$ given by Eq. (17), showing a symmetric Fano profile for $W = 0$ and an asymmetric Fano profile for $W = 2J$ [see also Figs. 5(b) and 5(d)]. We notice that at such weak-driving as $\Omega = J$ the peak (and the asymmetry) in the Fano profiles are suppressed with increasing density. However, for strong driving $\Omega \gg 4Jn_0$ we recover the features of complete reflection (complete transmission) through the impurity site as was already predicted by the linearization of the impurity.

C. Hard-core bosons

We now consider the limit of a strongly interacting Bose-gas. Its Hamiltonian is given by

$$\begin{aligned} H = & -J\sum_j (a_{j+1}^\dagger a_j + \text{H.c.}) + \frac{U}{2}\sum_j a_j^\dagger a_j^\dagger a_j a_j + \Delta |M\rangle\langle M| \\ & + \Omega(|M\rangle\langle Q|a_0 + a_0^\dagger |Q\rangle\langle M|) + W_Q a_0^\dagger |Q\rangle\langle Q| a_0 \\ & + W_M a_0^\dagger a_0 |M\rangle\langle M|, \end{aligned} \tag{63}$$

where the onsite-shift for two-bosons A on the same site U by far exceeds the tunneling rate J, i.e., $U \gg J$. Since double occupation of a site by two atoms A is strongly suppressed, we may eliminate those excitation from H, e.g. by imposing anticommutation relations for atoms on the same site, i.e., $(a_j)^2 = (a_j^\dagger)^2 \equiv 0$ and $\{a_j, a_j^\dagger\} = 1$. In the following we will focus on the limiting case $U/J \to \infty$, i.e., that of a Tonks gas. In this limit we may fermionize the Hamiltonian (63) via a Jordan-Wigner transformation (JWT) [26], which maps the commuting fields for the hard-core bosons, a_j, and the pseudo-spin of the impurity, $\sigma^- \equiv |M\rangle\langle Q|$, onto anticommuting fields, c_j and f, respectively. The JWT is given by

$$a_j = c_j \prod_{l<j} (1 - 2c_l^\dagger c_l), \quad a_j^\dagger = c_j^\dagger \prod_{l<j} (1 - 2c_l^\dagger c_l), \tag{64a}$$

$$\sigma^- = f \prod_l (1 - 2c_l^\dagger c_l), \quad \sigma^+ = f^\dagger \prod_l (1 - 2c_l^\dagger c_l). \tag{64b}$$

The fields c_j and f describe fermionic excitations for the new joint vacuum state of the system, $|\text{vac}\rangle_{CF} \equiv |Q\rangle|\text{vac}\rangle$. We rewrite the Hamiltonian (63) in terms of the fermionic excitations c_j and f and obtain

$$\begin{aligned} H = & -J\sum_{j<M} (c_{j+1}^\dagger c_j + \text{H.c.}) + \Delta f^\dagger f + \Omega(-1)^{\hat{N}_R}(f^\dagger c_0 + \text{H.c.}) \\ & + W_Q f f^\dagger c_0^\dagger c_0 + W_M f^\dagger f c_0^\dagger c_0, \end{aligned} \tag{65}$$

where $\hat{N}_R = \Sigma_{j>0} c_j^\dagger c_j = \Sigma_{j>0} a_j^\dagger a_j$ is the number of particles to the right of the impurity site. The Hamiltonian for the fermionic excitations, c_j and f, is the same as the one obtained for the Fermi gas, see Eq. (40), except for the appearance of the phase factor $(-1)^{\hat{N}_R}$ for the coupling Ω to the impurity.

We proceed by detailing the time-dependent scattering of a Tonks gas with N atoms A off the impurity atom Q. We assume that at time $t = 0$ the atoms A are trapped within a box of M sites to the left on impurity site. This corresponds to a Fermi-sea of the fermionic modes c_j, and the state of the system at $t = 0$ is given by (see also Sec. IV A)

$$\begin{aligned} |\Psi(0)\rangle &= \prod_{n=1}^N \left[\sqrt{\frac{2}{M+1}} \sum_{j<0} \sin(k_n x_j) c_j^\dagger \right] |\text{vac}\rangle_{\text{CF}} \\ &= |Q\rangle \sum_{\mathbf{j}<0} (-1)^{S(\mathbf{j})} \prod_{n=1}^N \left[\sqrt{\frac{2}{M+1}} \sin(k_n x_{j_n}) a_{j_n}^\dagger \right] |\text{vac}\rangle_A, \end{aligned} \tag{66}$$

where $k_n = n\pi/(M+1)a$ are the quasimomenta of the fermionic excitations, $\mathbf{j} = (j_1, j_2, \ldots, j_N)$ (with $j_p \neq j_q$) denotes the position of the N bosons, and $(-1)^{S(\mathbf{j})}$ the sign of the permutations of $\mathbf{j}$, i.e., $S(\mathbf{j}) = \Sigma_{j_p > j_q} 1$. Due to the cumbersomeness of the many-body wave function in terms of the bosonic operators a_j, it is preferable to deal within the fermionic picture and extract the quantities of interest from the correlations for the fermions. The density $n(x_j, t)$ of the hardcore bosons A corresponds to the density for the fermions c, while the correlations, $\rho(x_i, x_j, t)$, and the quasimomentum distribution of the Tonks gas, $n(k, t)$, differ from those of a Fermi gas, as

$$n(x_j, t) = \langle a_j^\dagger a_j \rangle_t = \langle c_j^\dagger c_j \rangle_t, \tag{67a}$$

$$\rho(x_i, x_j, t) = \langle a_i^\dagger a_j \rangle_t = \left\langle c_i^\dagger \prod_{l=i}^{j-1} [1 - 2c_l^\dagger c_l] c_j \right\rangle_t, \tag{67b}$$

$$n(k, t) = \frac{a}{2\pi} \sum_{p,q} e^{-ik(x_p - x_q)} \langle a_p^\dagger a_q \rangle_t = \frac{a}{2\pi} \sum_{p,q} e^{-ik(x_p - x_q)} \rho(x_p, x_q, t). \tag{67c}$$

We obtain the correlations and thereby also the quasimomentum distribution for the gas of hard-core bosons numerically, following the proceedings detailed in Refs. [27,28]: The correlation function can be rewritten as $\rho(x_p, x_q, t) = \langle \Phi_q(t) | \Phi_p(t) \rangle (-1)^{\delta_{p,q}} + \delta_{p,q}$ with $|\Phi_r(t)\rangle = c_r^\dagger \exp(i\pi \Sigma_{l<r} c_l^\dagger c_l) |\Psi(t)\rangle$ (for $r = p, q$), the overlap of two fermionic $(N+1)$ particle wave functions which differ by a unitary transformation and the position of the last excitation $c_r^\dagger$. We evaluate this quantity numerically as the determinant of a $(N+1) \times (N+1)$ matrix having as entries the overlaps of the single-particle wavefunctions of $\langle \Phi_q(t)|$ and $|\Phi_p(t)\rangle$. By

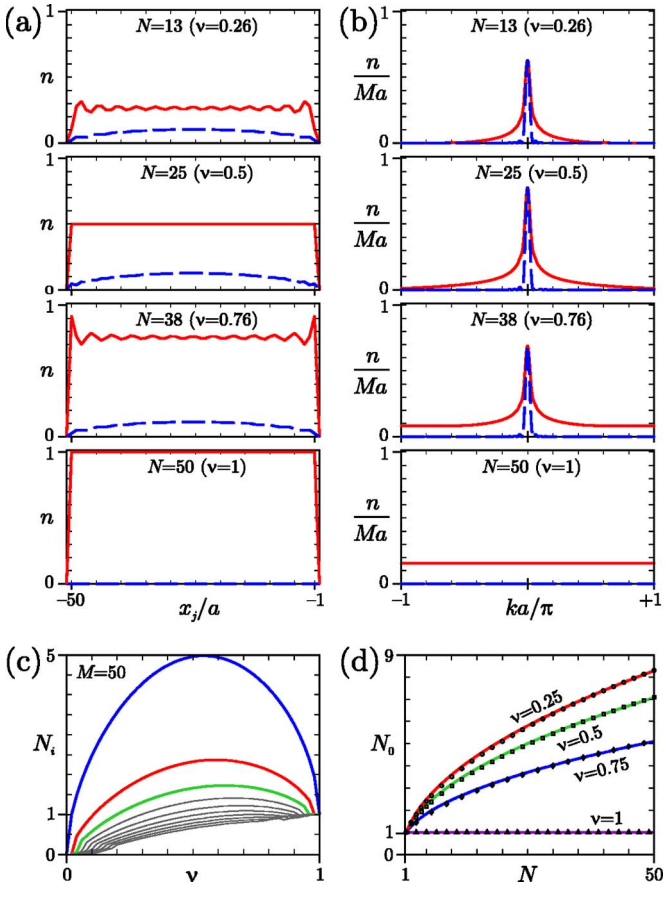

FIG. 13. (Color online) Initial density distribution of a gas of hard core bosons. (a),(b) Shown are the atomic density n (solid line) and the mode of the quasicondensate n_0 (dotted line) (a) in position space and (b) the corresponding momentum profiles. The gas is trapped on $M=50$ sites to the left of the impurity site, $x_j=0$, and for fillings factor $\nu=0.26,0.5,0.76,1$ (top to bottom). (c) The 10 largest eigenvalues N_i for the single particle density matrix as a function of the filling factor ν for a trap with $M=50$ sites. (d) The condensate fraction N_0 as a function of the particle number N for given filling $\nu=1/4,1/2,3/4,1$ shows the typical square-root scaling law.

diagonalizing the single-particle density matrix $\rho(x_i,x_j,t)$ for given time t one obtains the populations $N_i(t)$ of the various eigenmodes, in particular the condensate fraction $N_0(t)$ as the largest eigenvalue and the wavefunction of the quasicondensate $\psi_0(x_j,t)$ as the corresponding eigenmode. In the following we denote density of the quasicondensate by $n_0(x_j,t)=N_0(t)|\psi_0(x_j,t)|^2$ and its momentum distribution by $n_0(k,t)$.

In Figs. 13(a) and 13(b) we plot the initial densities profiles for a Tonks-gas trapped on $M=50$ sites as a function of the position and the momentum, respectively. Within each figure the filling factors are given by $\nu=0.26,0.5,0.76,1$ and correspond to $N=13,25,38,50$ particles (top to bottom insets). The solid lines in Fig. 13(a) show the densities in position space $n(x_j)$ while the dashed lines show the contribution of the largest eigenmode of the single-particle-density matrix $\rho(x_i,x_j)$, $n_0(x_j)$. In Fig. 13(b) we plot the corresponding quasimomentum distributions of the gas, $n(k)$ (solid line), and those of the largest eigenmode of $\rho(x_i,x_j)$, $n_0(k)$ (dashed line). The densities $n(x_j)$ correspond to that of a Fermi-gas trapped within a box with local filling factor ν, while the momentum distributions strongly differs from a Fermi sea (see insets of Fig. 8). In fact for incommensurate filling $\nu<1$ the momentum profiles show a sharp peak at $k=0$, which corresponds to the largest eigenmode of the system $n_0(k)$ (dashed lines), as one would expect for a condensate. With increasing filling factor ν the wings of this peak become significantly broader until the peak finally vanishes for commensurate filling $\nu=1$. There one attains a Mott insulator which has no phase coherence and therefore the momentum profile is flat as the corresponding Fermi profile. In Fig. 13(c) we plot the 10 larges eigenvalues of the single-particle densitiy matrix N_i as a function of the filling ν for $M=50$. We notice that the population of the quasicondensate N_0 increasing with the filling until it reaches near half filling its maximum of $N_0(\nu\approx 1/2)\simeq\sqrt{M/2}=\sqrt{N}$. For larger fillings the quasicondensates population then decreases until it is reduced to a single-particle $N_0=1$ for commensurate filling $\nu=1$. For fixed filling $0<\nu<1$ the condensed fraction of atoms in the system N_0 is known to be proportional to $\sqrt{N}$ particles [28]. To illustrate and verify this scaling-law we computed numerically the eigenvalues of the single-particle density matrix for up to $N=50$ particles for various fillings $\nu=0.26,0.5,0.76,1$, i.e., N particles trapped in a box of $M=N/\nu$ lattice sites. The markers in Fig. 13(d) show the number of particles in the quasicondensate N_0 obtained numerically, while the solid lines depict the square-root behavior as $f_\gamma(N)=\sqrt{\gamma(N-1)+1}\propto\sqrt{N}$ with the parameter γ fitted to the value of $N_0(\nu)$ for $N=51$.

We now describe the free ($\Omega=W_Q=0$) evolution of the Tonks gas after having opened the switch at $t=0$. From Eq. (65) we obtain the state of the system at time t as (see Sec. IV A)

$$|\Psi_t\rangle=|Q\rangle\prod_{n=1}^{N}\left[\sum_j \alpha_j(k_n,t)c_j^\dagger\right]|\text{vac}\rangle, \tag{68a}$$

$$\alpha_j(k_n,t)=\sqrt{\frac{2}{M+1}}\sum_{j'<0} U_{j,j'}(t)\sin(k_n x_j), \tag{68b}$$

where $U_{j,j'}(t)$ denotes the free single-particle propagator, cf. Eq. (38) with $W=\Omega=0$. The densities $n(x_j,t)$ of the hardcore-bosons A then correspond to that of the fermions, given by Eq. (43a), and are plotted in Fig. 14(a) for filling factors $\nu=0.26,0.5,0.76,1$ (top to bottom). Figure 14(b) shows the corresponding momentum distributions $n(k,t)$ for each filling factor ν. After opening the switch at $t=0$ the cloud starts to freely expand through the impurity site. Thereby the peak present at $k=0$ for incommensurate filling ($\nu<1$) for the momentum profile is broadened and slightly shifted towards a small $k_i>0$ with progressing time. For $t>0$ the bosons can disperse to the semi-infinite system, and start to condense into modes which have mean quasimomentum $k_d>0$. The condensation lasts until the cloud is significantly diluted at $t\approx J/M$. A signature of this process is that the momentum-distribution dynamical attains an additional (initially broader) peak, which is centered at $k_d>k_i$ [see, e.g.,

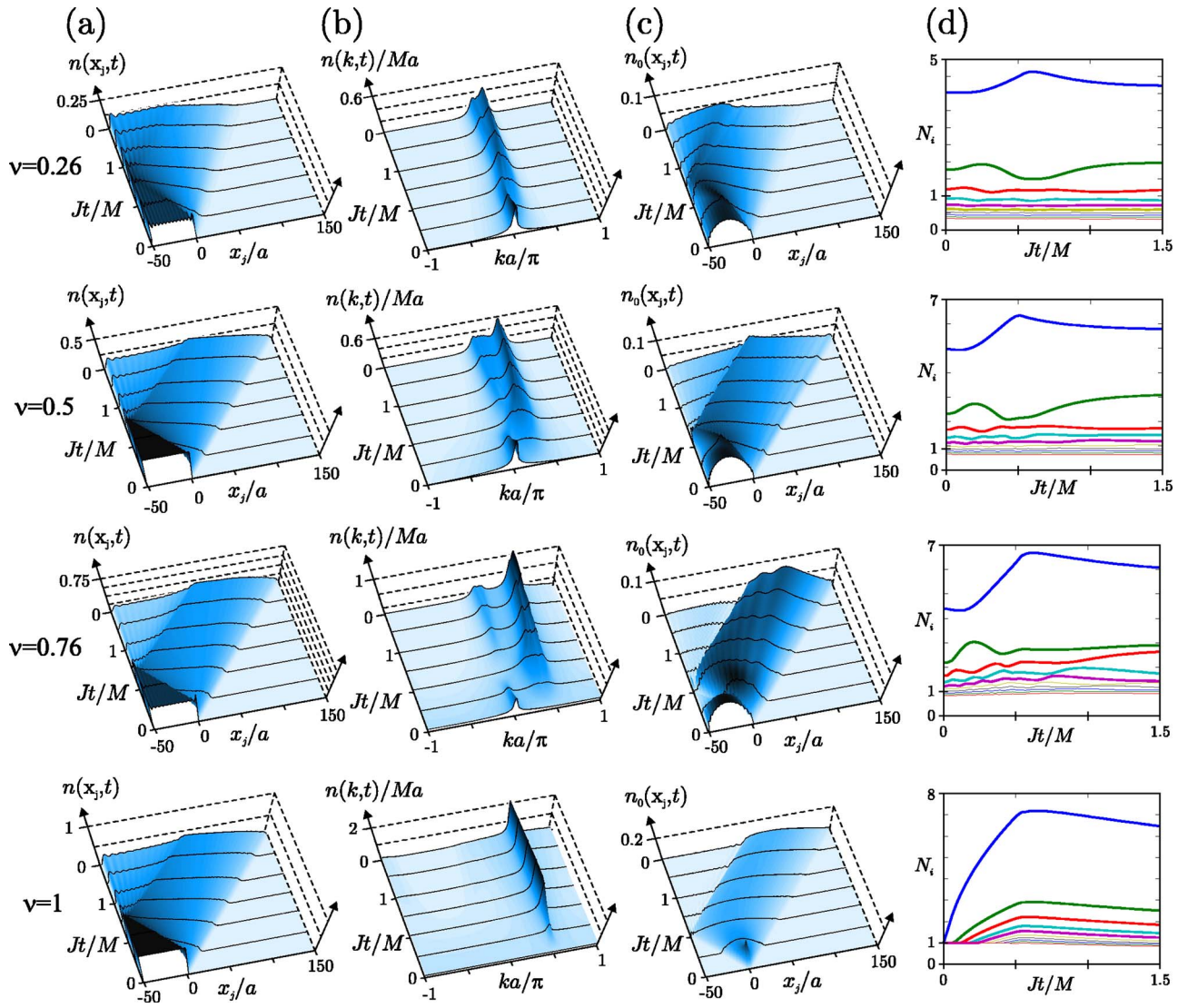

FIG. 14. (Color online) Free evolution of a gas of hard core bosons. The gas is initially trapped on $M=50$ to the left of the impurity site, $x_j=0$, and the fillings factor is given by $\nu=0.26,0.5,0.76,1$ (top to bottom). Shown are the atomic density n as a function of (a) the position x_j, (b) the momentum k, and (c) the quasicondensate density $n_0(x_j,t)$ after opening the mirror at $t=0$. (d) The largest 10 eigenvalues of the system $N_i(t)$ as a function of time show the growth of the population of the quasicondensate $N_0(t)$ for each filling ν (solid line).

Fig. 14(b) at $t=M/2J$]. This peak corresponds to a quasicondensate which propagates coherently to the right with mean quasimomentum $k_d>0$ [27]. The density of this quasicondensate $n_0(x_j,t)$ is plotted in Fig. 14(c) for each filling factor ν. The value of the mean quasimomentum of the quasicondensate k_d can be obtained by considering the conservation of energy within the system [27] as follows: Assume that all N particles were to condense into a single monochromatic mode with $k=k_d$. In this case the initial cloud had an total energy $E_{\text{tot}}=-2J\Sigma_{n=1}^{N}\cos(k_n a)$, and thus the quasimomentum would be given by $k_d=\arccos(E_{\text{tot}}/2JN)/a>0$. The value of k_d depends on the initial filling factor, see Fig. 14(b). In particular $k_d\to 0$ for $\nu\to 0$ and k_d increases with ν. It attains its maximum, $k_d=\pi/2a$, for commensurate filling $\nu=1$. There one has zero initial energy $E_{\text{tot}}=0$ and the quasimomentum attains the maximal group-velocity $v=2Ja$. Figure 14(d) shows the evolution of the 10 largest eigenvalues of the single particle density matrix, $N_i(t)$. We see that the number of particles in the quasicondensate (solid line) grows for $t>0$. It saturates to $N_0\propto\sqrt{N}$ [27] at $t\sim Jt/2M$, when the density of atomic cloud is strongly diluted. For larger times the condensed fraction N_0 stays almost constant, as the dynamically established quasi-condensate decays only very slowly [27].

In the presence of a finite on-site shift $W_Q\neq 0$, but with driving $\Omega=0$, the Hamiltonian is still bilinear in the fermionic modes $c_i^\dagger$ and c_j. The evolution of the system is given by Eq. (68), but now with $U_{j',j}(t)$ being the single-particle propagator for $W\neq 0$. In Figs. 15(a)–15(c) we show the evolution of a Tonks gas with $\nu=1/2$ for $W=0$, $W=J$ and $W=2J$, respectively. On the left side we plot the density distribution $n(x_j,t)$ in the middle the momentum distribution $n(k,t)$, and to the right the quasicondensate $n_0(x_j,t)$. Darker regions correspond to regions of higher density. For no interaction $W=0$ the particles freely tunnel through the impurity. The momentum distribution is shifted towards $k>0$ as well

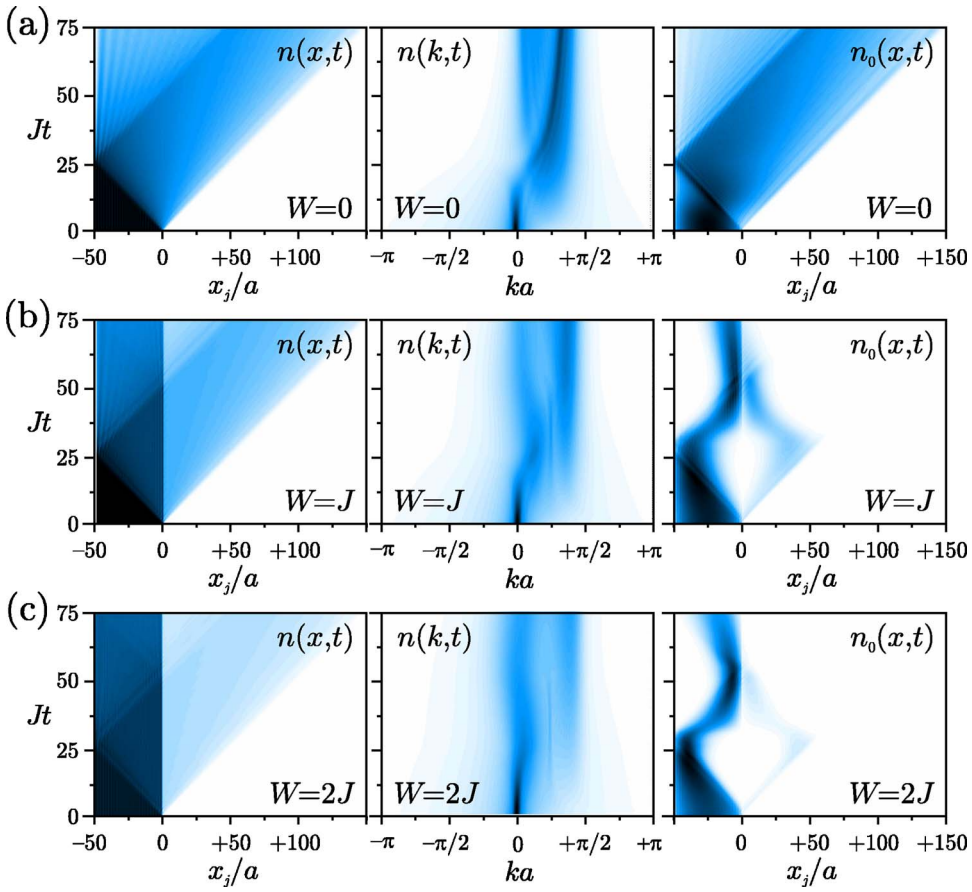

FIG. 15. (Color online) Evolution of a gas of hard-core bosons with filling factor $\nu=1/2$ for $\Omega=0$ and (a) $W=0$, (b) $W=J$, (c) $W=2J$. Shown are the density $n(x_j,t)$ (left column), the momentum distribution $n(k,t)$ and the density of the quasicondensate $n_0(x_j,t)$.

as being broadened. At $t\approx M/2J=25/J$ an additional peak in the momentum distribution is formed at $k_d\approx 0.35\pi/a$, which corresponds to the mode of the quasicondensate $n_0(x_j,t)$, tunneling through the impurity, see Fig. 15(a). For $W=J$ the tunneling of particles through the impurity site is partially blocked and the dynamical formation of a monochromatic mode with $k_d>0$ is suppressed, see Fig. 15(b). Thereby the condensate mode $n_0(x_j,t)$ remains mainly localize to the left side of the impurity. For $W=2J$ only a small fraction of atoms passes through the impurity and the momentum distribution remains centered at $k=0$, although it becomes slightly broader, see Fig. 15(c). In fact the condensed fraction of atoms in the condensate is efficiently hindered from passing the impurity and remains localized to the left of the impurity site.

In the presence of a finite coupling $\Omega>0$, the Hamiltonian is no more bilinear in $c_j^\dagger$ and c_j, due the appearance of the nonlinear factor $(-1)^{\hat{N}_R}=\Pi_{j>0}(1-2c_j^\dagger c_j)$, which makes a description of the time-dependent scattering in terms of the fermionic modes c_j in the general case as difficult as integrating out the full many-body Schrödinger equation (63) for the hard-core bosons A. However, the contribution of the nonlinear factor $(-1)^{\hat{N}_R}$ to the dynamics is negligible for strong driving $\Omega\gg J,|\Delta|,W$, and also for low densities $\nu\ll 1$. In this case the number of atoms on the right $N_R(t)\ll 1$, and thus we set $\hat{N}_R\to 0$ in Eq. (65). The state of the system is given by

$$|\Psi_t\rangle=\prod_{n=1}^{N}\left[\sum_j \alpha_j(k_n,t)c_j^\dagger+\beta(k_n,t)f^\dagger\right]|\mathrm{vac}\rangle, \tag{69a}$$

$$\alpha_i(k_n,t)=\sqrt{\frac{2}{M+1}}\sum_{j<0}U_{i,j}(t)\sin(k_n x_j), \tag{69b}$$

$$\beta(k_n,t)=\sqrt{\frac{2}{M+1}}\sum_{j<0}U_{M,j}(t)\sin(k_n x_j), \tag{69c}$$

where $U_{\alpha,j}(t)$ denotes the full single-particle propagator, cf. Eq. (38). In this regime the density distribution of the Tonks-gas, $n(x_j,t)$, corresponds to that of a Fermi gas (see e.g. the left side in Fig. 8).

For the general case of many bosons A, arbitrary coupling strengths, and even finite U, we refer to the exact numerical simulation given in Ref. [24]. These simulations allow one to test the behavior of the gas for essentially arbitrary repulsion U and density ν, i.e., for the full crossover regime from a weakly interacting dilute Bose-gas up to a dense Tonks gas.

V. CONCLUSION

We have studied a scheme utilizing quantum interference to control the transport of atoms in a 1D optical lattice by a single impurity atom. The two internal state represent a qubit (spin-1/2), which in one spin state is perfectly transparent to

the lattice gas, and in the other spin state acts as a single atom mirror, confining the lattice gas. This allows us to "amplify" the state of the qubit, and provides a single-shot quantum non-demolition measurement of the state of the qubit. We have derived exact analytical expression for the scattering of a single atom by the impurity, and gave approximate expressions for the dynamics a gas of many interacting bosonic of fermionic atoms. A numerical study of this dynamics based on time-dependent DMRG techniques, which complements the present discussion, is presented in Ref. [24].

ACKNOWLEDGMENTS

The authors acknowledge helpful discussion with A. Daley and D. Jaksch. Work in Innsbruck is supported by the Austrian Science Foundation, EU Networks, and the Institute for Quantum Information.

APPENDIX A: SCATTERING OF GAUSSIAN WAVE PACKETS

We consider the dynamics of a bosonic N-particle state of the form

$$|\Psi_t\rangle = \frac{1}{\sqrt{N!}}\left[\sum_j \alpha_t(x_j)a_j^\dagger + \beta_t b^\dagger\right]^N|\mathrm{vac}\rangle,$$

where at $t=0$ the Gaussian wave packet is given by $\beta_0=0$ and

$$\alpha_0(x_j) = \mathcal{N}_0 e^{-\delta k_0^2(x_j-x_0)+ik_0x_j},$$

where $x_0 \ll 0$ ($k_0>0$) is the mean position (momentum) and $\delta k_0 < \pi/a$ the width in momentum space at $t=0$. For $\delta k_0 \ll \pi/a$ we may take the continuum limit $\Sigma_j \to \int dx/a$ and obtain $\mathcal{N}_0 \approx (2\delta k_0^2 a^2/\pi)^{1/4}$, and $\delta x_0 \approx 1/2\delta k_0 \gg a/\pi$. The momentum representation is given by

$$\tilde{\alpha}_0(k) = (a/2\pi)^{1/2}\sum_j e^{-i*k*x_j}\alpha_0(x_j) \approx (2\pi\delta k_0^2)^{-1/4}e^{-(k-k_0)^2/4\delta k_0^2 - i(k-k_0)x_0}.$$

1. Molecular density

For the evolution we are interested at the population of the molecular state, which follows as

$$n_m(t) = \langle b^\dagger b\rangle_t = N\left|\sum_j U_{M,j}(t)\alpha_0(x_j)\right|^2 = N\mathcal{N}_0^2\left|\sum_j U_{M,j}(t)e^{-\delta k_0^2(x_j-x_0)+ik_0x_j}\right|^2,$$

where $U_{M,j}(t)=\langle M|e^{-iHt}|j\rangle$ is the single particle propagator. We introduce the peak of the initial atomic density $n_0 \equiv n(x_0,t=0)=N\mathcal{N}_0^2 \approx N(2/\pi)^{1/2}\delta k_0 a$.

For the scattering off the particles, i.e., for $|x_0| \gg r_B$, we may neglect the finite range of the bound state and have

$$n_m(t) \approx N\left|\sum_j \frac{a}{2\pi}\int dk e^{-iE_kt}\frac{\Omega t_k}{E_k-\Delta}e^{ik|x_j|}\alpha_0(x_j)\right|^2 = N\left(\frac{a}{2\pi}\right)\left|\int dk e^{-iE_kt}\frac{\Omega t_k}{E_k-\Delta}\tilde{\alpha}_0(k)\right|^2.$$

Thus we have $n_m(t)=n_0|f_t|^2$ with

$$f_t = \frac{1}{2\delta k_0\sqrt{\pi}}\int dk \frac{\Omega t_k}{E_k-\Delta}e^{-iE_kt-[(k-k_0)/2\delta k_0]^2-i(k-k_0)x_0}.$$

For the Fourier transform we use a saddle-point method, however, we have to distinguish which one is narrower, either the width of the wave packet δk_0, or the width of dressing profile.

2. Broad Fano profile

For a broad resonance, i.e., $\Omega t_k/(E_k-\Delta)$ slowly varying on the Bloch band we expand the integral around $k \approx k_0$, i.e., with $E_k \approx E_0 + v_0(k-k_0)+(k-k_0)^2/2m_0$ and $\Omega t_k/(E_k-\Delta) \approx \Omega t_0/(E_0-\Delta)$, where energy $E_0 \equiv E_k|_{k=k_0}$, velocity $v_0 \equiv \partial E_k/\partial k|_{k=k_0}$, and effective mass $m_0 \equiv 1/(\partial^2 E_k/\partial^2 k)|_{k=k_0}$. Notice that $m_k=-1/a^2E_k$ for the explicit shape of the Bloch-band and choice of the origin in the band middle.

Thereby we obtain

$$n_m(t) = n_0\frac{\delta k_t}{\delta k_0}e^{-2\delta k_t x_t^2}\mathcal{D}_0,$$

where the linear propagation, spreading and dressing are

$$x_t = x_0 + v_0 t,$$

$$\delta k_t = \frac{\delta k_0}{\sqrt{1+(2\delta k_0^2 a^2 E_0 t)^2}},$$

$$\mathcal{D}_0 = \left.\frac{\Omega^2|t_k|^2}{(E_k-\Delta)^2}\right|_{k=k_0} = \frac{\Omega^2}{(E_0-\Delta)^2+[\Omega^2+W(E_0-\Delta)]^2a^2/v_0^2}.$$

We notice that at $t_\star = -x_0/v_0 = |x_0/v_0|$ we attain a maximal molecular density of

$$n_m(t_\star) = n_0\frac{\mathcal{D}_0}{\sqrt{1+(2\delta k_0^2 a^2 E_0 t)^2}}.$$

For $E_0 \approx 0$ we might neglect the broadening/spreading. We recognize that $\mathcal{D}_0$ is maximal for such detuning Δ and initial momentum k_0 where

$$E_\star \approx \Delta - W\frac{\Omega^2}{W^2+v_\star^2/a^2},$$

is on the bloch band. This corresponds to the position of the Fano profile. As $v_\star^2/a^2 = 4J^2 - E_\star^2$ the equation for $E_\star$ is implicitly cubic gives the same recursive equation. Thus the maximal density for a broad resonance $\Omega \gg |J-\Delta|$ is suppressed as

$$n_m(t_\star) \approx n_0\frac{v_0^2/a^2}{\Omega^2}, \tag{A1}$$

while far off resonance $|\Delta| \gg \Omega$ we have

$$n_m(t_\star) \approx n_0 \frac{(\Omega/\Delta)^2}{1+(aW/v_0)^2}. \tag{A2}$$

3. Narrow Fano profile

In the second case, that of a narrow resonance, i.e., a sharp Fano profile, we have that the dressing factor is narrower than the Gaussian wave packet, hence we approximate via a Saddle-point method. We expand the dressing function

$$\mathcal{D}_k = \frac{\Omega t_k}{E_k - \Delta} = \left[\frac{ia\Omega}{v_k} + \frac{E_k - \Delta}{\Omega}\left(1 + \frac{iaW}{v_k}\right)\right]^{-1},$$

around the momentum $k_\star$ where $|\mathcal{D}_k|$ is maximal,

$$\mathcal{D}_k \approx C_0 e^{+iC_1(k-k_\star)a-(1/2)C_2(k-k_\star)^2a^2}, \tag{A3}$$

with

$$C_0 = \frac{-i\Omega}{\zeta},$$

$$C_1 = \frac{\gamma_\star + iW}{\zeta} - \frac{im_\star}{\gamma_\star}\left(1 + i\frac{E_\star - \Delta}{\zeta}\right),$$

$$C_2 = \left(\frac{\gamma_\star + iW}{\zeta}\right)^2 - \frac{im_\star}{\gamma_\star}\left(\frac{\gamma + iW}{\zeta} + \frac{2\Omega^2}{a^2}\right) + \frac{m_\star^2}{\gamma_\star^2}\left[1 + \frac{(E_\star - \Delta)^2}{\zeta^2}\right],$$

$$\zeta \equiv \frac{\Omega^2 + (E_\star - \Delta)(W - i\gamma_\star)}{\gamma_\star},$$

where $E_\star = E(k_\star)$, $\gamma_\star = \partial E(k)/\partial ka|_{k=k_\star} = v(k_\star)/a$, $m_\star = \partial^2 E(k)/\partial(ka)^2 = -E(k_\star)$ are the lowest expansion coefficient of the dispersion relation $E(k) = -2J\cos(ka)$ at $k = k_\star$.

The position of its maximum $k_\star$ is obtained from the expansion (A3) by requiring $\mathrm{Im}[C_1] = 0$ with

$$\mathrm{Im}[C_1] = \gamma_\star \frac{\Omega^2 W + (E_\star - \Delta)(\gamma_\star^2 + W^2)}{\Omega^4 + 2(E_\star - \Delta)\Omega^2 W + (E_\star - \Delta)(\gamma_\star^2 + W^2)} - \frac{m_\star}{\gamma_\star}\frac{[\Omega^2 + (E_\star - \Delta)W]^2}{\Omega^4 + 2(E_\star - \Delta)\Omega^2 W + (E_\star - \Delta)(\gamma_\star^2 + W^2)}.$$

In the limit of interest (i.e., near the middle of the Bloch band), we have $|m_k/\gamma_k| = |\cot(ka)| \ll 1$ thus we obtain the energy of the maximum as a series

$$E_\star \approx \Delta - \frac{W\Omega^2}{\gamma_\star^2 + W^2} + \frac{m_\star \gamma_\star^2 \Omega^4}{(\gamma_\star^2 + W^2)^3} + O^2(m_\star). \tag{A4}$$

Since $\gamma_\star$, $m_\star = -E_\star$ all depend on $k_\star$ the series gives implicitly the value of $k_\star$. Moreover, we notice that the truncation to first order in $m_\star$ yields the exact result for $W = 0$.

Then with

$$\zeta \approx \frac{\Omega^2}{\gamma_\star - iW}\left[1 - i\frac{m_\star}{\gamma_\star}\left(\frac{\Omega\gamma_\star}{W^2 + \gamma_\star^2}\right)^2\right],$$

$$C_0 \approx \frac{-(W + i\gamma_\star)/\Omega}{1 - im_\star\gamma_\star\Omega^2/(\gamma_\star^2 + W^2)^2},$$

$$C_1 \approx \frac{\gamma_\star^2 + W^2}{\Omega^2} - \frac{m_\star W}{\gamma_\star^2 + W^2},$$

$$C_2 \approx \left(\frac{\gamma_\star^2 + W^2}{\Omega^2}\right)^2 - i\frac{m_\star}{\gamma_\star}\frac{\gamma_\star^2 - W^2 - 4i\gamma_\star W}{\Omega^2}, \tag{A5}$$

we can compute the Fourier-integral and obtain

$$|f_t|^2 = |C_0|^2 |A(t)| e^{-(1/2)\mathrm{Re}[A(t)(2\delta k_0 x(t) + ik_0 - k_\star/\delta k_0)^2 + (k_0 - k_\star/\delta k_0)^2]},$$

$$A(t) = [1 + 2\delta k_0^2 a^2 (C_2 + im_\star t)]^{-1},$$

$$x(t) = x_0 + v_\star t - aC_1. \tag{A6}$$

For $E_\star \approx 0$, i.e., near the middle of the Bloch band, we might neglect the spreading of the wave packet, i.e., $m_\star \approx 0$. Then we have

$$|C_0|^2 = C_1 = \frac{W^2 + v_\star^2/a^2}{\Omega^2} = \sqrt{C_2},$$

$$|f(t)|^2 = \frac{C_1 \exp\left[-\dfrac{2\delta k_0^2 x(t)^2 + C_1^2 (k_0 - k_\star)^2 a^2}{1 + 2\delta k_0^2 a^2 C_1^2}\right]}{1 + 2\delta {k_0}^2 a^2 C_1^2}. \tag{A7}$$

In the limit $\Omega \to 0^+$ the probability $|f(t)|^2$ vanishes as

$$\max_t |f(t)|^2 \approx \frac{\Omega^2}{W^2 + v_\star^2/a^2} \frac{\exp\left[-\dfrac{(k_0 - k_\star)^2}{2\delta k_0^2}\right]}{2\delta {k_0}^2 a^2}. \tag{A8}$$

APPENDIX B: VARIATIONAL ANSATZ

For the ansatz (60) we obtain the action (61) as

$$S = \frac{1}{2}\sum_\sigma \left[c_\sigma^* \frac{\partial c_\sigma}{\partial t} - \Delta\delta_{\sigma M}|c_\sigma|^2 + N_\sigma |c_\sigma|^2 \sum_j \alpha_{j,\sigma} \times \left(i\frac{\partial \alpha_{j,\sigma}}{\partial t} + J\alpha_{j+1,\sigma} + J\alpha_{j-1,\sigma} - W\delta_{j0}\alpha_{j,\sigma}\right)\right] - \Omega\sqrt{N} c_M^* c_Q \left(\sum_j \alpha_{j,M}^* \alpha_{j,Q}\right)^N \alpha_{j,Q} + \mathrm{c.c.},$$

with $c_\sigma \equiv c_\sigma(t)$, $\alpha_{j,\sigma} \equiv \alpha_{j,\sigma}(t)$ and $N_Q = N_M + 1 = N$.

Minimizing the action S with respect to c_σ^* and $\alpha_{j,\sigma}$, we obtain after some algebra,

$$ic_M^* \frac{\partial c_M}{\partial t} = \Delta|c_M|^2 + \lambda - (N-1)\frac{\lambda + \lambda^*}{2},$$

$$ic_Q^* \frac{\partial c_Q}{\partial t} = \lambda^* - N\frac{\lambda + \lambda^*}{2},$$

with the effective coupling $\lambda=\Omega\sqrt{N}c_M^* c_Q s^{N-1}\alpha_{0,Q}$ and

$$i|c_M|^2\frac{\partial\alpha_{j,M}}{\partial t}=|c_M|^2\left(-J\sum_{\pm}\alpha_{j\pm1,M}+W\delta_{j0}\alpha_{j,M}\right)-\frac{\lambda-\lambda^*}{2}\alpha_{j,M}+\frac{\lambda}{s}\alpha_{j,Q},$$

$$i|c_Q|^2\frac{\partial\alpha_{j,Q}}{\partial t}=|c_Q|^2\left(-J\sum_{\pm}\alpha_{j\pm1,Q}+W\delta_{j0}\alpha_{j,Q}\right)+\frac{\lambda-\lambda^*}{2}\alpha_{j,Q}+\frac{N-1}{N}\frac{\lambda^*}{s^*}\alpha_{j,M}+\frac{\lambda^*\delta_{j0}}{N\alpha_{0,Q}^*}$$

where the overlap s is given by $s=\Sigma_j\alpha_{j,M}^*\alpha_{j,Q}$.

[1] C. Cohen-Tannoudji, J. Dupont-Roc, and G. Grynberg, *Atom-Photon Interactions: Basic Processes and Applications*, Wiley Science Paperback Series (Wiley, New York, 1992).

[2] J. McKeever, A. Boca, A. D. Boozer, R. Miller, J. R. Buck, A. Kuzmich, and H. J. Kimble, Science **303**, 1992 (2004).

[3] G. Nogues, A. Rauschenbeutel, S. Osnaghi, M. Brune, J. M. Raimond, and S. Haroche, Nature (London) **400**, 239 (1999).

[4] P. Maunz, T. Puppe, I. Schuster, N. Syassen, P. W. H. Pinkse, and G. Rempe, Nature (London) **428**, 50 (2004).

[5] S. Rinner, H. Walther, and E. Werner, Phys. Rev. Lett. **93**, 160407 (2004).

[6] For a review see, e.g., D. Jaksch and P. Zoller, Ann. Phys. (N.Y.) **315**, 52 (2005).

[7] M. Greiner, O. Mandel, T. Esslinger, T. W. Hansch, and I. Bloch, Nature (London) **415**, 39 (2002).

[8] O. Mandel, M. Greiner, A. Widera, T. Rom, T. W. Hansch, and I. Bloch, Phys. Rev. Lett. **91**, 010407 (2003).

[9] T. Stöferle, H. Moritz, C. Schori, M. Köhl, and T. Esslinger, Phys. Rev. Lett. **92**, 130403 (2004).

[10] E. L. Bolda, E. Tiesinga, and P. S. Julienne, Phys. Rev. A **66**, 013403 (2002).

[11] R. Ciurylo, E. Tiesinga, and P. S. Julienne, Phys. Rev. A **71**, 030701(R) (2005).

[12] M. Holland, J. Park, and R. Walser, Phys. Rev. Lett. **86**, 1915 (2001).

[13] M. Theis, G. Thalhammer, K. Winkler, M. Hellwig, G. Ruff, R. Grimm, and J. H. Denschlag, Phys. Rev. Lett. **93**, 123001 (2004).

[14] A. Recati, P. O. Fedichev, W. Zwerger, J. von Delft, and P. Zoller, Phys. Rev. Lett. **94**, 040404 (2005).

[15] R. B. Diener, B. Wu, M. G. Raizen, and Q. Niu, Phys. Rev. Lett. **89**, 070401 (2002).

[16] V. B. Braginsky and F. Y. Khalili, *Quantum Measurement* (Cambridge University Press, Cambridge, 1992).

[17] See, for example, G. Johansson, P. Delsing, K. Bladh, D. Gunnarsson, T. Duty, A. Käck, G. Wendin, and A. Aassime, e-print cond-mat/0210163.

[18] A. Micheli, A. J. Daley, D. Jaksch, and P. Zoller, Phys. Rev. Lett. **93**, 140408 (2004).

[19] D. Jaksch, C. Bruder, J. I. Cirac, C. W. Gardiner, and P. Zoller, Phys. Rev. Lett. **81**, 3108 (1998).

[20] S. Datta, *Electronic Transport in Mesoscopic Systems* (Cambridge University Press, Cambridge, 1997).

[21] G. D. Mahan, *Many Particle Physics*, 3rd ed. (Plenum, New York, 2000).

[22] L. S. Levitov, in *Quantum Noise in Mesoscopic Physics*, edited by Y. V. Nazarov (Kluwer, Dordrecht, 2002).

[23] M. A. Cazalilla and J. B. Marston, Phys. Rev. Lett. **88**, 256403 (2002), and references cited therein.

[24] A. Daley, S. R. Clark, D. Jaksch, P. Zoller, Phys. Rev. A **72**, 043618 (2005).

[25] M. Lukin, Rev. Mod. Phys. **75**, 457 (2003).

[26] See, for example, S. Sachdev, *Quantum Phase Transitions* (Cambridge University Press, Cambridge, 1999).

[27] M. Rigol and A. Muramatsu, Phys. Rev. Lett. **93**, 230404 (2004).

[28] M. Rigol and A. Muramatsu, Phys. Rev. A **70**, 031603(R) (2004); **72**, 013604 (2005), and references cited therein.